DR CARLOS MARTINEZ-SALGADO (Orcid ID : 0000-0003-4641-6717)

Article type : Regular Paper

Cardiotrophin-1 opposes renal fibrosis in mice: Potential prevention of chronic kidney disease

Nuria Perretta-Tejedor[1,2,3], José M. Muñoz-Félix[1,3], Annette Düwel[1,2,3], Yaremi Quiros-Luis[1], José Luis Fernández-Martín[4], Ana I. Morales[1,3], Francisco J. López-Hernández[1,2,3], José M. López-Novoa[1,3], Carlos Martínez-Salgado[1,2,3,*]

[1]Translational Research on Renal and Cardiovascular Diseases (TRECARD), Department of Physiology and Pharmacology, University of Salamanca, Salamanca, Spain. [2]Institute of Health Sciences Studies of Castilla y Leon (IECSCYL). [3]Institute of Biomedical Research of Salamanca (IBSAL), Salamanca, Spain. [4]UGC Bone Metabolism, Institute of Health Research of the Principality of Asturias (ISPA), Oviedo, Asturias, Spain.

Short title: Cardiotrophin-1 and renal fibrosis

*Correspondence to:

Carlos Martínez-Salgado

Departamento de Fisiología y Farmacología, Edificio Departamental

This article has been accepted for publication and undergone full peer review but has not been through the copyediting, typesetting, pagination and proofreading process, which may lead to differences between this version and the Version of Record. Please cite this article as doi: 10.1111/apha.13247

Plaza Doctores de la Reina s/n, Campus Miguel de Unamuno

37007 Salamanca, Spain

Phone: +34923294500 ext. 1945. Fax: +34923294669

Email: carlosms@usal.es

ABSTRACT

Aim: Chronic kidney disease is characterized by tubulointerstitial fibrosis involving inflammation, tubular apoptosis, fibroblast proliferation and extracellular matrix accumulation. Cardiotrophin-1, a member of the interleukin-6 family of cytokines, protects several organs from damage by promoting survival and anti-inflammatory effects. However, whether cardiotrophin-1 participates in the response to chronic kidney injury leading to renal fibrosis is unknown.

Methods: We hypothesized and assessed the potential role of cardiotrophin-1 in a mice model of tubulointerstitial fibrosis induced by unilateral ureteral obstruction.

Results: Three days after unilateral ureteral obstruction, obstructed kidneys from cardiotrophin-$1^{-/-}$ mice show higher expression of inflammatory markers IL-1β, Cd68, ICAM-1, COX-2 and iNOs, higher activation of NF-κB, higher amount of myofibroblasts and higher severity of tubular damage and apoptosis, compared with obstructed kidneys from wild-type littermates. In a later stage, obstructed kidneys from cardiotrophin-$1^{-/-}$ mice show higher fibrosis than obstructed kidneys from wild-type mice. Interestingly, administration of exogenous cardiotrophin-1 prevents the increased fibrosis resulting from the genetic knock-out of cardiotrophin-1 upon unilateral ureteral obstruction, and supplementation of wild-type mice with exogenous cardiotrophin-1 further reduces the renal fibrosis induced by unilateral ureteral obstruction. In vitro, renal myofibroblasts from cardiotrophin-$1^{-/-}$ mice have higher collagen I and fibronectin expression and higher NF-κB activation than wild-type cells.

Conclusions: Cardiotrophin-1 participates in the endogenous response that opposes renal damage by counteracting the inflammatory, apoptotic and fibrotic processes. And exogenous cardiotrophin-1 is proposed as a candidate for the treatment and prevention of chronic renal fibrosis.

Keywords: apoptosis, cardiotrophin-1, inflammation, myofibroblasts, renal fibrosis, unilateral ureteral obstruction.

INTRODUCTION

Chronic kidney disease (CKD) is a serious condition of progressive and irreversible renal damage known to affect 10% of the adult population and to lead to end-stage renal disease, which requires renal replacement therapy (in the form of dialysis or kidney transplantation) to preserve life, with a disproportionate cost [1,2]. CKD is characterized by a progressive decrease in nephron number and glomerular filtration rate that eventually lead to renal failure [3]. Tubulointerstitial fibrosis, a key pathophysiological element of CKD is characterized by tubular cell apoptosis followed by tubular atrophy, inflammatory cell infiltration including lymphocytes and macrophages, excessive deposition of extracellular matrix (ECM) in the renal interstitium possibly due to fibroblast accumulation [4] and peritubular microvasculature rarefaction, leading to tissue scarring [3]. At present, there are no effective treatments, because renal fibrosis is a complex and irreversible process [5,6]. Therefore, it is important to improve our knowledge on the key cellular and molecular mechanisms of the disease and to identify new strategies to prevent renal fibrosis. Recent research focuses on new therapeutic strategies aimed at inhibiting key mediators in the progression of renal fibrosis, including angiotensin II or transforming growth factor beta 1 (TGF-β1) [1,6].

Cardiotrophin-1 (CT-1) is a member of the interleukin-6 (IL-6) family of cytokines originally identified as a hypertrophic factor for neonatal ventricular cardiomyocytes through the JAK/STAT pathway. CT-1 signaling starts by binding and activating the cell surface receptors glycoprotein 130 (gp130) and

leukemia inhibitory factor receptor (LIFR) [7]. *CT-1* mRNA is expressed in several tissues including the heart, lung, kidney, brain, liver and skeletal muscle [8]. CT-1 has a protective effect in several organs, as it promotes survival of cardiomyocytes [9,10] and neurons [11], and exerts antiapoptotic effects in different experimental models of liver, renal and neuronal damage [12-15]. In addition, administration of CT-1 provides protection against ischaemia/reperfusion liver damage [16], hepatic failure [17] and hepatitis of viral origin [18]. Moreover, CT-1 knockout mice are more sensitive to liver damage induced by ischaemia/reperfusion [16]. Some reports have shown that CT-1 attenuates the expression of pro-inflammatory cytokines such as IL-1β, tumor necrosis factor alpha (TNF-α), adhesion molecules intercellular adhesion molecule 1 (ICAM-1), vascular cell adhesion molecule 1(VCAM-1), inducible nitric oxide synthase (iNOs) and CD68 in several models of tissue damage, including endotoxemia, [19] orthotropic liver transplant [15] and renal ischaemia/reperfusion injury via nuclear factor (NF)-κB inhibition [13]. Also in rats, CT-1 administration prevents contrast nephropathy [20] and gentamicin nephrotoxicity [21]. There are no data yet about the effect of endogenous CT-1 in the development of tubulointerstitial fibrosis and renal damage.

We hypothesized and analyzed a role for CT-1 as a natural defense of the kidney against the development of tubulointerstitial fibrosis in the unilateral ureteral obstruction (UUO) experimental model, in CT-$1^{-/-}$ and wild type (WT) mice. We also analyzed cultured renal fibroblasts and tubular epithelial cells derived from WT and CT-$1^{-/-}$ mice to evaluate the in vitro expression of CT-1 and its cell receptors and the role of CT-1 after TGF-β1 induced ECM protein expression in renal myofibroblast, as TGF-β1 is the main profibrotic cytokine involved in tubulointerstitial fibrosis [22].

RESULTS

CT-1 deficiency increases tubulointerstitial fibrosis, parenchymal damage, apoptosis and renal inflammation

The participation of CT-1 in the endogenous response to renal damage was studied by comparing the renal fibrosis induced by UUO in WT and CT-1 KO mice. After 15 days of UUO, obstructed kidneys in both WT and CT-$1^{-/-}$ mice show the typical features of obstructive nephropathy: tubular dilatation, hydronephrosis and tubulointerstitial damage, whereas contralateral, non obstructed kidneys show the normal characteristics of the renal parenchyma (Suppl. Fig. 1A-B). We observed that obstructed kidneys from CT-$1^{-/-}$ mice have a higher degree of fibrosis than obstructed kidneys from WT mice, as supported by more extensive areas of collagen (i.e. Sirius red, Fig. 1A and Suppl. Fig 2A) and fibrotic material deposition (i.e. Masson's trichrome, Fig.1B and Suppl. Fig 2B), collagen I mRNA (Fig. 1C), total collagen content (Fig. 1D), and collagen I, fibronectin and connective tissue growth factor (CTGF) accumulation (Fig. 1E). All these data show that CT-1 deficiency increases UUO-induced tubulointerstitial renal fibrosis.

Tubular cell injury and apoptosis, interstitial inflammation and myofibroblasts abundance are the key initial molecular mechanisms promoting kidney injury and renal fibrosis in the UUO experimental model [23]. Hematoxylin-eosin staining shows that non obstructed kidneys from WT and CT-$1^{-/-}$ have normal renal parenchyma (Suppl. Fig. 2C). Tubular damage of 3 days-obstructed kidneys, characterized by tubular cell swelling, brush border loss, loss of nuclei in the tubules or tubular dilatation, was more severe in obstructed kidneys from CT-$1^{-/-}$ than in obstructed kidneys from WT mice (Fig. 2A and Suppl. Fig 3A).

Apoptosis is the most prevalent type of cell death in UUO [24,25] appearing from the first day after UUO and increasing with time [26]. Apoptosis was analyzed by cleaved caspase-3 (an executor caspase) expression and by TUNEL staining. 3 days-obstructed kidneys from CT-1$^{-/-}$ mice show significantly higher expression of cleaved caspase-3 than obstructed kidneys from WT mice, assessed by Western blot and by immunohistochemistry (Fig. 2B-C respectively). In agreement, 3 days-obstructed kidneys from CT-1$^{-/-}$ mice show a significantly higher number of TUNEL-stained cells in both the cortex and corticomedular areas than obstructed kidneys from WT mice (Fig. 2D). Moreover, 3 days-obstructed kidneys from WT mice show significantly higher STAT3 phosphorylation than obstructed kidneys from CT-1$^{-/-}$ mice (Fig. 2E), which might be related with the reduced apoptosis observed in WT mice.

Myofibroblasts are responsible for the synthesis and deposition of ECM proteins being key effectors in renal fibrosis [27]. We evaluated myofibroblast abundance by analyzing the expression of the myofibroblast markers α-smooth muscle actin (α-SMA) and vimentin (analyzed by Western blot and immunohistochemistry).

Three days-obstructed kidneys from CT-1$^{-/-}$ mice show higher α-SMA expression than obstructed kidneys from WT mice (Fig. 2F). α-SMA is expressed in the vessel walls and in the renal interstitium, whereas vimentin is also expressed in mesangial cells; however, 3 days-obstructed kidneys from CT-1$^{-/-}$ mice show higher vimentin and α-SMA expression in the interstitial area that obstructed kidneys from WT mice (Fig. 2G). Assuming that this stained area is proportional to the number of myofibroblasts, our data suggest that the increase in myofibroblast number is higher in obstructed kidneys from CT-1$^{-/-}$ mice than in obstructed kidneys from WT mice.

Tubulointerstitial fibrosis is conditioned by infiltration of inflammatory cells (predominantly macrophages and leukocytes) and local expression of different cytokines (such as TNF-α), chemokines and membrane adhesion molecules [3]. In the UUO model, interstitial inflammatory cell

infiltration progressively increases 12 h after obstruction [28]. Adhesion molecules expression (such as ICAM-1 and VCAM-1) is increased just a few hours after UUO and mediate chemotaxis and adhesion of macrophages [29]. Moreover, iNOs overexpression is a characteristic hallmark of the inflammatory state and its expression is upregulated in response to pro-inflammatory cytokines [30]. COX-2 induction can occur in response to cytokines during tissue damage or inflammation [31]. We observed that 3 days-obstructed kidneys from CT-$1^{-/-}$ mice show significantly higher expression of Cd68 mRNA (a macrophage marker) than obstructed kidneys from WT mice (Fig. 3A). Three days-obstructed kidneys from CT-$1^{-/-}$ mice also show significantly higher expression of ICAM-1 and COX-2 (Fig. 3B). iNOs expression was evaluated by Western blot (Fig. 3C) and immunohistochemistry (Fig. 3D); 3 days-obstructed kidneys from CT-$1^{-/-}$ mice show significantly higher expression of iNOs than obstructed kidneys from WT mice; immunohistochemistry analysis show iNOs expression in the cellular cytoplasm, mainly in the cortical tubules.

NF-κB is activated after renal obstruction [32,33] and its activation is thought to be essential for the induction of iNOs [34,35]. The inhibition of NF-κB activity prevents obstruction-induced renal fibrosis [36]. Activation of NF-κB was assessed by analyzing the expression of the phosphorylated Ser536 residue in NF-κB p65 subunit (pp65) and the free IκB-α levels. Three days-obstructed kidneys from CT-$1^{-/-}$ mice show significantly higher expression of pp65 and IκB-α than obstructed kidneys from WT mice (Fig. 3E).

All these data suggest that CT-1 deficiency aggravates the early phases of UUO-induced tubular damage, myofibroblasts abundance and presence of inflammatory mediators.

Administration of exogenous CT-1 prevents the increased fibrosis resulting from the genetic knock-out of CT-1 upon UUO

In order to verify that specifically CT-1 deficiency, and not an undetermined artefact derived from genetic manipulation, is indeed responsible for the effects observed in the previous experiments, CT-1 was administered to CT-1 KO mice subject to UUO. CT-1 administration reduces interstitial collagen deposition in 15 days-obstructed kidneys from CT-$1^{-/-}$ mice, according to Masson´s trichrome and Sirius red staining (Fig. 4A and Suppl. Fig 3B). Quantification of Sirius red staining shows that 15 days-obstructed kidneys from CT-1 treated mice have significantly less renal fibrotic area than obstructed kidneys from control mice (Fig. 4A). In agreement with these results, CT-1 administration reduces collagen I and fibronectin mRNA expressions (Fig. 4B) as well as collagen I and fibronectin protein expressions (Fig. 4C) in CT-$1^{-/-}$ mice. CT-1 administration reduces α-SMA and PCNA expressions (Fig. 4D). Immunofluorescence analysis show that α-SMA is expressed in the vessel walls and in the renal interstitium, however CT-1 treated 15 days-obstructed kidneys show lower α-SMA expression in the renal interstitium that non-treated obstructed kidneys (Fig. 4E). Moreover, immunochemistry for vimentin show that 15 days-obstructed kidneys from CT-1 treated mice have lower vimentin expression in the renal interstitium than obstructed kidneys from non-treated mice (Fig. 4F), thus suggesting that the increase in myofibroblast number is higher in non-treated kidneys than in CT-1 treated kidneys from CT-$1^{-/-}$ mice, and that CT-1 administration also reduces the degree of renal fibrosis after 15 days of UUO.

We also evaluated the effect of CT-1 administration in the early stages of tubulointerstitial disease. Hematoxylin-eosin staining shows that CT-1 administration significantly ameliorates tubular damage induced by 3 days-UUO in CT-$1^{-/-}$ mice (Fig. 5A-B and Suppl. Fig. 3C). 3 days-obstructed kidneys from CT-1 treated mice show lower cleaved caspase-3 expression than obstructed kidneys from non-treated mice, as observed by Western blot (Fig. 5C) and immunohistochemistry (Fig. 5D). CT-1 administration also reduces the number of TUNEL-positive cells in both cortex and corticomedular areas (Fig. 5E). 3 days-obstructed kidneys from CT-$1^{-/-}$ mice treated with CT-1 show lower vimentin (Fig. 5F) and α-SMA (Fig. 5G-H) expression in the renal interstitium than obstructed kidneys from

non-treated mice. Moreover, CT-1 administration reduces Cd68 mRNA and IL-1β mRNA expression in 3 days-obstructed kidneys (Fig. 6A). CT-1 administration also reduces the expression of VCAM-1, IκB-α and COX-2 (Fig. 6B). iNOs immunostaining analysis showed that non treated 3 days-obstructed kidneys show a higher iNOs expression than CT-1 treated obstructed kidneys (Fig. 6C), suggesting that CT-1 administration reduces iNOs expression. All these data show that supplementation of CT-1 levels ameliorates the tubular damage and apoptosis, inflammatory response and myofibroblasts abundance observed after 3 days UUO in CT-1$^{-/-}$ mice.

Our results indicate that CT-1 plays a significant role in the response of the organism to oppose or repair damage, or both. They also show that exogenous CT-1 mimics the effects of endogenous CT-1.

Treatment with exogenous CT-1 further ameliorates UUO-induced renal fibrosis in WT mice

We next studied the effect of administration of exogenous CT-1 to WT mice after UUO, with the purpose of knowing whether maximal effect was achieved by the endogenous CT-1 and, if not, whether a therapeutic opportunity exists by supplementing CT-1 to prevent renal fibrosis. 15 days-obstructed kidneys from CT-1 treated mice at both doses (100 and 400 μg kg^{-1} b.w.) show significantly lower interstitial collagen deposition than obstructed kidneys from non-treated mice (Fig. 7A and Suppl. Fig. 4A). 15 days-obstructed kidneys from CT-1 treated mice have significantly less renal area occupied by fibrosis than obstructed kidneys from non-treated mice (Fig. 7A and Suppl. Fig. 4A). Moreover, CT-1 treatment reduces CTGF and fibronectin expression (Fig. 7B). These data suggest that CT-1 administration reduces the degree of renal fibrosis after 15 days of UUO also in WT mice.

CT-1 administration at both doses (100 and 400 μg kg^{-1} b.w.) significantly reduces tubular damage (Fig. 8A, B and Suppl. Fig. 4B), the expression of cleaved caspase-3 (Fig. 8C, D) as well as the number

of TUNEL-positive cells in both the cortex and corticomedular area (Fig. 8E) in 3 days-obstructed kidneys. CT-1 also significantly reduces the expression of α-SMA, PCNA (Fig. 8F and Suppl. Fig. 4C) and vimentin expression in the renal interstitium (Fig. 8G). Regarding the expression of inflammatory mediators, CT-1 administration significantly reduces Cd68 and IL-1β mRNA expression (Fig. 9A), as well as protein expression of the cell adhesion molecule ICAM-1 and COX-2 (Fig. 9B). CT-1 administration also reduces iNOs expression (Fig. 9C). On the other hand, the amount of pp65 and IκB-α is higher in non-treated 3 days-obstructed kidneys than in CT-1 treated obstructed kidneys (Fig. 9B). All these data indicate that CT-1 administration ameliorates the early tubular damage and apoptosis, as well as the inflammatory response and myofibroblast abundance induced by UUO during three days in WT mice.

UUO upregulates CT-1 expression

Because CT-1 seems to act in response to renal damage, it is reasonable to wonder whether CT-1 is overexpressed by damaged kidneys, or whether CT-1-mediated effects rely on a housekeeping level of this cytokine. To shed light into this issue, we assessed CT-1 expression in the kidney (Suppl. Fig. 4D). There is a higher expression of CT-1 mRNA in obstructed than in non obstructed kidneys after 15 days of UUO, as assessed by qPCR (Fig. 10A). Immunohistochemistry analysis shows higher CT-1 staining in obstructed kidneys than in non obstructed kidneys after 15 days of UUO, and this higher CT-1 expression is mainly observed in the tubular epithelium (Fig. 10B). Therefore, our results demonstrate that CT-1 is upregulated in kidneys after UUO.

CT-1 is expressed in tubular epithelial cells and myofibroblasts, and its deficiency modulates ECM synthesis and NF-κB pathway

Both myofibroblasts (Fig. 10C-D) and tubular epithelial cells (Fig. 10E) express CT-1 and its receptors gp130 and LIFR (Fig. 10F-G). Moreover, stimulation with 40 ng mL^{-1} CT-1 for 15 minutes induces STAT3 phosphorylation in both cell types (Fig. 10H-I). CT-$1^{-/-}$ renal myofibroblasts show a higher expression of collagen I and fibronectin both in basal conditions and after TGF-β1 stimulation (1 ng mL^{-1}) than WT renal fibroblasts (Fig. 10J). On the other hand, CT-1 KO renal myofibroblasts show more pp65 and IκB-α expression than WT fibroblasts, either in basal conditions or after TGF-β1 stimulation (Fig. 10K). These *in vitro* results support our *in vivo* findings showing that CT-1 KO mice have a higher degree of fibrosis than WT mice.

DISCUSSION

In the UUO model, an experimental model of tubulointerstitial fibrosis that replicates many features of obstructive nephropathy [37], renal fibrosis was exacerbated in mice lacking CT-1, accompanied by increased inflammation, cell apoptosis and myofibroblast accumulation. These findings provide the first evidence that endogenous CT-1 modulates tubulointerstial damage.

Renal fibrosis is likely initiated as a result of a failed or altered response to tubular injury. For unknown reasons, the restorative process losses the appropriate regulation and efficacy, which leads to scarring of deficiently repaired structures and to a pathologic vicious cycle of tissue damage and tubulointerstial fibrosis [2]. The increased CT-1 expression observed after UUO is congruent with CT-1 acting as an endogenous defence mechanism activated to repair or counteract tubular injury, providing a protective effect against renal damage and fibrosis. Congruently with this, we previously reported that plasma levels of CT-1 correlate with early renal damage (i.e. as evidenced by

microalbuminuria and elevated albumin/creatinine ratio) in hypertensive and diabetic patients [38]. All in all, these findings propose CT-1 as a protective tissue barrier, as a potential biomarker of renal repair and, by extension, as a surrogate marker of renal fibrosis.

The effect of CT-1 is probably due to its capacity to target multiple mechanisms involved in the development of UUO-induced renal fibrosis [39], including epithelial tubular cell apoptosis, monocyte-macrophage infiltration, abnormal deposition of ECM components, and tubule-interstitial inflammation [23,37]. During the development of renal fibrosis, tubular cell apoptosis plays a key role promoting the progression of disease in terms of contributing to the inflammatory response and regulating fibroblasts abundance [23,26]. JAK/STAT3 is one of the main signaling pathways activated by CT-1 [39], and STAT3 activation provides resistance to apoptosis through the induction of Bcl-xl [40,41]. In our study the higher vulnerability of CT-1 deficient mice to UUO-induced apoptosis is associated to a lower activation of STAT3, and CT-1 stimulation induced STAT3 phosphorylation in cultured myofibroblasts and tubular epithelial cells, thus pointing at STAT3 activation as one of the pathways involved in the antiapoptotic role of CT-1. In agreement with our results, CT-1 KO mice undergo more apoptosis than WT mice after liver injury, due to a reduction in STAT3 phosphorylation [16]. And the JAK/STAT3 signalling pathway plays a key role in the repair process of UUO-induced renal fibrosis via MMP-2 activation [42].

Oxidative stress is increased in the obstructed kidney [34, 43,44] and mediates renal inflammatory damage after UUO [45]. Oxidative stress induces CT-1 expression in hepatocytes [16] and cardiomyocites [46] in which a hypoxic conditioned medium has enhanced ability to activate STAT3 [47]. So this increased oxidative stress may be responsible of the increased CT-1 expression observed in the damaged kidney. Oxidative stress activates NF-κB, a typical feature of renal obstruction [11,48]. NF-κB induces the expression of genes encoding proinflammatory cytokines (IL-1, TNF-α), chemokines (MCP1, Rantes), adhesion molecules (ICAM-1, VCAM-1), and inducible enzymes (COX-2 and iNOs),

thus enhancing the inflammatory response in the obstructed kidney [34,49-51]. We hypothesize that the oxidative stress produced in the early stages after UUO leads to an increased expression of CT-1 in the damaged kidney, which increases STAT3 activation. In turn, STAT3 reduces oxidative stress and prevents NF-κB activation leading to a reduction in ICAM-1, VCAM-1, COX-2 and iNOs expression, which contributes to a reduced macrophage infiltration and overall inflammatory response. This is in agreement with the effect of CT-1 in other organs. In fact, CT-1 administration reduces oxidative stress after injury in the heart [52], liver [16] and kidney [13,20], through the activation of gp130/STAT3, which in turn increases the expression of Mn-SOD, thus scavenging superoxide anion through its transformation into the less damaging H_2O_2, as it was described in cardiomyocytes after ischaemia/reperfusion injury [53].

The higher degree or renal fibrosis observed in CT-1 KO mice may represent a secondary effect of enhanced apoptosis, macrophage infiltration, inflammation and myofibroblasts accumulation. In this case, the lack of CT-1 implies a lower restorative effect after UUO which leads to a worsening of the disease. Our results obtained after CT-1 administration support this hypothesis. Treatment with additional (i.e. exogenous) CT-1 not only prevents the effects produced by knocking the CT-1 gene, but it also affords extra protection to WT mice by further decreasing the severity of renal fibrosis. This effect results both from efficiently ameliorating early UUO-induced tubulointerstitial damage (tubular injury, apoptosis, inflammation, presence of myofibroblasts), and the later excessive ECM deposition.

Summarizing, endogenous CT-1 opposes and ameliorates the initial damage induced by obstructive nephropathy acting as a protective mechanism against cell apoptosis, inflammation and renal fibrosis. While the endogenous CT-1 is not enough to restore all the UUO-induced damage, exogenous administration of CT-1 provides additional protection by potentiating the same mechanisms activated by endogenous CT-1. Our results propose CT-1 treatment as a new candidate

for ameliorating the tubulointerstitial fibrosis induced by obstructive nephropathy by potentiating an endogenous repair and defence mechanism. This poses an alternative, but complementary strategy to approaches aiming at inhibiting pro-fibrotic mediators and mechanisms. Although chronic exposure to high levels of CT-1 induces renal fibrosis in healthy rats [54], these damaging effects are due to the maintenance of high CT-1 doses over long periods of time, because none of these effects have been observed when this cytokine is administered for short periods or in low doses [55]. In clinical perspective, CT-1 has been approved for human use by the US Food and Drug Administration (FDA) with the status of orphan drug as it protects the liver for ischaemia/reperfusion injury due to the transplantation procedure (designation request 07–2449) and for acute liver failure treatment (designation request 11–3507). The same status has been granted by the European Medicines Agency (EMA) for the prevention of ischemic/reperfusion injury associated with solid organ transplantation (EU/3/06/396). Moreover, there is a clinical trial in the US with healthy volunteers to assess the tolerability, safety and pharmacokinetics of CT-1 (registered at https://clinicaltrials.gov/; identifier NCT01334697, checked on February 2017). All these data and circumstances make CT-1 a promising candidate for its clinical use against renal fibrosis and other diseases related to alterations in its expression or activity.

METHODS

Experimental in vivo model of tubulointerstitial fibrosis

Generation of CT-1$^{-/-}$ mice was previously described [11]. A breeding colony of adult CT-1$^{-/-}$ mice has been maintained in the pathogen-free facilities for genetically modified mice under controlled ambient conditions (Animal Experimentation Service, University of Salamanca, Spain) in a temperature-controlled room with a 12 hours light / dark cycle, and were reared on standard chow (Panlab, Barcelona, Spain) and water ad libitum. Mice were backcrossed with C57BI/6 mice for nine

generations. Routine genotyping of DNA isolated from mouse tail biopsies was performed by PCR using these primers: for CT-1 forward 5-TGACTCCATGGTCCTTTGGC-3′ and reverse 5′-GACGGTGATAGGGGCTTGTC-3′; for NEO cassette forward 5′- AGCCGATTGTCTGTTGTGCCC-3′and reverse 5′-AGCAAGTGGATCTCTATGAGCTG-3′. UUO has been performed as previously described [56]. 10 week old mice were anesthetized with Isoflurane (Schering-Plough, Madrid, Spain), the abdomen was closed with running sutures and the skin was sewn with interrupted sutures. UUO was maintained during 3 and 15 days. In all procedures, mice were treated in accordance with the Declaration of Helsinki Principles on the Advice on Care and Use of Animals referred to in: law 14/2007 (3 July) on Biomedical Research, Conseil de l'Europe (published in Official Daily N. L358/1-358/6, 12/18/1986), Spanish Government (Royal Decree 223/1988, (14 March) and Order of 10/13/1989, and Official Bulletin of the State b. 256, pp. 31349–31362, 10/28/1990). The procedure was approved by the Bioethics committee of the University of Salamanca. We performed 6 experimental designs and 16 experimental groups to carry out the study:

- Consequences of the absence of CT-1 after 15 days of UUO. 2 groups: CT-$1^{-/-}$ (n=6) and WT mice (n=6).
- Consequences of the absence of CT-1 after 3 days of UUO. 2 groups: CT-$1^{-/-}$ (n=6) and WT mice (n=6).
- Effect of CT-1 administration in CT-$1^{-/-}$ mice after 15 days of UUO. 3 groups: mice receiving 100 µg kg^{-1} CT-1 iv (n=5), mice receiving 400 µg kg^{-1} CT-1 iv (n=5) and mice receiving saline solution (n=6) every 2 days after UUO.
- Effect of CT-1 administration in CT-$1^{-/-}$ mice after 3 days of UUO. 3 groups: mice receiving 100 µg kg^{-1} CT-1 iv (n=5), mice receiving 400 µg kg^{-1} CT-1 iv (n=6) and mice receiving saline solution (n=6) the day after UUO.

- Effect of CT-1 administration in WT mice after 15 days of UUO. 3 groups: mice receiving 100 μg kg^{-1} CT-1 iv (n=5), mice receiving 400 μg kg^{-1} CT-1 iv (n=5) and mice receiving saline solution (n=6) every 2 days after UUO.
- Effect of CT-1 administration in WT mice after 3 days of UUO. 3 groups: mice receiving 100 μg kg^{-1} CT-1 iv (n=5), mice receiving 400 μg kg^{-1} CT-1 iv (n=6) and mice receiving saline solution (n=6) the day after UUO.

Recombinant murine CT-1 was supplied by Peprotech (London, UK). CT-1 doses were selected based on previous studies showing CT-1 renoprotective effects [13,20,21]

Renal tissue preparation

Obstructed (O) and contralateral non obstructed (NO) kidneys were extracted and perfused with heparinized saline solution 3 or 15 days after UUO surgery. Kidneys were halved longitudinally, one half for protein and RNA extraction and total collagen measurement and the other half for histological studies. Renal samples for protein and RNA extraction and total collagen measurements were frozen in liquid nitrogen and stored at -80ºC. Renal samples for histological studies were fixed during 24 h in formaldehyde and then embedded in paraffin.

Cell culture

Renal myofibroblasts were obtained from obstructed kidneys of 10 weeks old WT and CT-$1^{-/-}$ mice 3 days after UUO, as it has been previously described [57-59]. Kidneys were washed with saline solution (NaCl 0.9%) and Dulbecco solution (2.6mM KCl, 1.5mM KH_2PO_4, 137mM NaCl, 8mM Na_2HPO_4, 5.6mM glucose) supplemented with 500U mL^{-1} penistreptomycin. Kidneys were cut in thin slices (0.2mm) with a sterile scalpel and were embedded in a 0.45 mg L^{-1} collagenase type IA (Sigma-

Aldrich, St Louis, MO, USA) solution for 40 min at 37ºC. Supernatant was placed in several plates in Dulbecco's modified Eagle's medium (Gibco, Life Technologies, Carlsbad, CA, USA) containing 10% fetal calf serum (FCS) and 100U mL^{-1} penicillin/streptomycin at 37ºC, in the presence of 5% CO_2. Cells expressed the typical myofibroblast marker smooth muscle α-actin (Suppl. Fig. 5A), and did not express the epithelial cell marker e-cadherin and cytokeratin (data not shown), as it has been previously described [59,60]. In the third passage, when cultures achieved 80–90% confluence, cells were serum starved for 24 h before performing the experiments. Cells were stimulated with 40 ng mL^{-1} CT-1 and 1 ng mL^{-1} TGF-β1 (R&D Systems, Minneapolis, MN, USA) for 15 min or 24 h.

Tubular epithelial cells were obtained from kidneys of 10 weeks old WT and CT-$1^{-/-}$ mice, as it has been previously described, with some modifications [61]. Kidneys were washed with saline solution (NaCl 0.9%) and Dulbecco solution supplemented with 500U mL^{-1} penistreptomycin. Renal cortex was cut in thin slices (0.2mm) with a microtome; slices were embedded in a 1.5 mg mL^{-1} collagenase type IA (Sigma-Aldrich) solution for 30 min at 37ºC. The solution was passed through a 250 µm sieve, centrifuged at 400g during 2 minutes and the pellet was resuspended in a 50% Percoll solution and 50% Krebs 2x solution (112.7 mM NaCl, 3.3 mM KCl, 1.2 mM PO_4H_2K, 1.2 mM $MgSO_47H_2O$, 0.5mM $CaCl_2$). After centrifugation at 35000g during 30 minutes, proximal tubules were recovered and washed with Dulbecco solution. Supernatant was placed in several plates in Advanced DMEM-F12 medium (Molecular Probes, Barcelona, Spain) containing 10% FCS, 12.5mM HEPES, 2.5mM L-glutamine, 1% non-essential amino acids, 1% ITS, 100 µg mL^{-1} EGF and 100U mL^{-1} penicillin/streptomycin at 37ºC, in the presence of 5% CO_2. Cells expressed the epithelial cell marker e-cadherin and pan-cytokeratin (Suppl. Fig. 5B), as it has been previously described [61]. In the third passage, when cultures achieved 80–90% confluence, cells were serum starved for 24 h before performing the experiments. Cells were stimulated with 40 ng mL^{-1} CT-1 for 15 min.

Western blot

Total cell extracts and tissue protein extracts were homogenized in lysis buffer (150 mmol L^{-1} NaCl, 1% IGEPAL CA-630, 10 mmol L^{-1} $MgCl_2$, 1 mmol L^{-1} EDTA, 10% glycerol, 1 mmol L^{-1} Na_3VO_4, 25 mmol L^{-1} NaF, 1 mmol L^{-1} phenylmethanesulfonylfluoride, 10 mg mL^{-1} aprotinin, and 10 mg mL^{-1} leupeptin) containing 25 mmol L^{-1} HEPES, pH 7.5, for renal tissue and magnesium lysis buffer (MLB, from Millipore, Billerica, MA, USA) supplemented with 80% glycerol, 1 mg mL^{-1} leupeptin, 1 mg mL^{-1} aprotinin, 10mM phenylmethanesulfonylfluoride, 1mmol L^{-1} Na_3VO_4, and 25 mmol L^{-1} NaF for cells, and centrifuged at 14000 g during 20 min. Supernatants were recovered and the protein amount was quantified. Lysates were separated by electrophoresis in 10–15% acrylamide gels (Mini Protean II system, Bio-Rad, Madrid, Spain). Immediately, proteins were electrically transferred to an Immobilon-P membrane (Millipore, Billerica, MA, USA). Membranes were probed with the following primary antibodies: rat anti-cardiotrophin-1 and goat anti-ICAM-1/CD54 (RD System, dilution 1:1000), rabbit anti-fibronectin (Millipore; 1:1000), goat anti-CTGF (L-20), goat anti-COX-2 (C-20), rabbit anti-iNOs/NOS2 (N-20), rabbit anti-IKB-α (C-21) and goat anti-VCAM-1 (C-19) (Santa Cruz Biotechnology, Madrid, Spain; 1:1000), rabbit anti-collagen I (Chemicon International, Temecula, CA, USA; 1:1000), mouse anti-GAPDH (Ambion, Barcelona, Spain; 1:50000), mouse anti-α-SMA (Sigma-Aldrich; 1:4000), mouse anti-PCNA (Transduction Laboratories, Madrid, Spain; 1:1000), rabbit anti-p-NF-κB p65, rabbit anti-p-STAT3 and rabbit anti-cleaved caspase-3 (Cell Signaling, Barcelona, Spain; 1:1000). Membranes were incubated with the corresponding horseradish peroxidase-conjugated secondary antibodies (1:10000) and were developed using ECL chemiluminescence reagent (Amersham Biosciences, Barcelona, Spain). Developed signals were recorded on X-ray films (Fujifilm Spain, Barcelona, Spain) for densitometric analysis (Scion Image Software, Frederick, MD, USA).

PCR analysis

For RT-PCR analysis, total RNA was isolated using Nucleospin RNAII (Macherey-Nagel, Cultek, Madrid, Spain), according to the manufacturer's instructions. Single-strand cDNA was generated from 400 ng of total RNA using iScript RT Supermix 5X (Bio-Rad). Quantitative RT-PCR was performed in triplicate. Each 20 µL reaction contained 1 µL of cDNA, 400 nM of each primer, and 1x iQ SybrGreen Supermix (Bio-Rad). Standard curves were run for each transcript to ensure exponential amplification and to rule out non-specific amplification. Gene expression was normalized to ribosomal protein S13 (rps13) expression. The reactions were run on an iQ5 Real-time PCR detection system (Bio-Rad). Primers used were: For mouse rps13: forward 5´ - GATGCTAAATTCCGCCTGAT - 3´ and reverse 5´-TAGAGCAGAGGCTGTGGATG-3´; for mouse IL-1β forward 5´-GCCTGTGTTTTCCTCCTTGC-3´ and reverse 5´-TGCTGCCTAATGTCCCCTTG-3´; for mouse Cd68 forward 5´-GGGGCTCTTGGGAACTACAC-3´ and reverse 5´-GTACCGTCACAACCTCCCTG-3´ ; for mouse collagen I 5´-GGAGAGAGCATGACCGATGGA-3´ and reverse 5´-GGTGGACATTAGGCGAGGAA-3´; for mouse fibronectin forward 5´-TGACAGTTGGGTCACCCTGTT-3´ and reverse 5´-GGTGTCTGGGTGACTTTCCT-3´ and for mouse CT-1 (primePCR assay qMmuCID0020747 Bio-Rad). Cycling conditions for fibronectin, rps13 and IL-1β: 95ºC, 5 min, 35 cycles of 1 min 95ºC, 1 min 59ºC and 1 min 72ºC, and an elongation cycle of 5 min 72ºC. Cycling conditions for collagen I: 95ºC, 5 min, 35 cycles of 1 min 95ºC, 1 min 56ºC and 1 min 72ºC, and an elongation cycle of 5 min 72ºC. Cycling conditions for Cd68: 95ºC, 5 min, 35 cycles of 1 min 95ºC, 1 min 60ºC and 1 min 72ºC, and an elongation cycle of 5 min 72ºC. Cycling conditions for CT-1: 95ºC, 2min, 40 cycles of 5 sec 95ºC, 30 sec 60ºC and a melt curve cycle between 65-95ºC 5 sec/step.

Total collagen determination

Kidneys were removed as previously described. Isolation and concentration of total collagen was performed using the kidney sample with acid neutralizing reagent (0.5M acetic acid, 0.1 mg mL^{-1} pepsin) (Sigma-Aldrich) and collagen isolation and concentration reagent (Biocolor, Northern Ireland, U.K.) and centrifuged at 12000 rpm, 4°C, 10 min. Then, the pellets were resuspended with Sircol Dye reagent (Biocolor) and proceed with the Sircol Soluble Collagen Assay according to the manufacturer instructions to measure all acid-soluble and pepsin-soluble collagens.

Histochemistry and immunohistochemistry

Three μm slices were cut from paraffin-embedded tissues and were stained with Sirius red, hematoxylin–eosin staining, and Masson's trichrome. Sirius red staining was quantified by Image-Pro Plus software (Media Cybernetics, Bethesda, MD, USA), and 15 randomly chosen renal cortical areas from each sample were analyzed. Immunohistochemical analysis was performed on buffered formalin-fixed, paraffin-embedded tissues as previously described [59]. Briefly, 3μm sections were deparaffinized in xylene and rehydrated in graded ethanol before staining with the peroxidase–antiperoxidase method. Endogenous peroxidase was blocked by incubation in 3% hydrogen peroxide. Primary antibodies were: rabbit anti-cleaved caspase-3 (Cell Signaling, dilution 1:100), rat anti-cardiotrophin-1 (RD System, dilution 1:100), rabbit anti-iNOs/NOS2 (N-20) (Santa Cruz Biotechnology, dilution 1:100) and rabbit anti-vimentin (EP21) (Cell Marque, Sigma-Aldrich; dilution 1:100). After three washes in phosphate-buffered saline (PBS: 0.81% NaCl, 2.6mM H_2KPO_4, and 4.1mM HNa_2PO_4), sections were sequentially incubated with the Novolink Polymer Detection System (Novocastra, Newcastle, UK) using 3,30-diaminobenzidine (Biogenez, San Ramón, CA, USA) as chromogen. Sections were lightly counterstained with hematoxylin and were dehydrated and cover-slipped. Negative controls were prepared without primary antibodies. Images were photographed

using an Olympus BX51 microscope connected to an Olympus DP70 colour, digital camera (Olympus, Tokyo, Japan).

After hematoxylin–eosin staining, tubular injury was determined by means of a "total severity score," which was calculated semiquantitatively in a blind analysis. Briefly, 10 fields per cortical renal slice were examined under light microscopy (magnification: ×400). Each field was divided into 10 sections. A score of 0–3 was assigned to each section, according to the following criteria: 0, normal histology; 1, tubular cell swelling, brush border loss, nuclear condensation, loss of nuclei in the tubules or tubular dilatation in up to one third of the section; 2, same as for 1, but from one third to two third of the section; and 3, same as for 1 but from two to three third of the section. Section scores were added to give a field score (maximal score per field = 30). The average score of 10 fields was used for each kidney sample.

Immunofluorescence

Paraffin-embedded tissues were cut in 3 μm sections. Heat-induced antigen unmasking was performed in 10mM Tris–1mM EDTA, pH 8.00, and washed with PBS. Sections were incubated with mouse anti-α-SMA (Sigma-Aldrich; dilution 1:100) for 1 h at room temperature. Following three washes in PBS, sections were incubated with goat anti-mouse CY3 (Jackson Immunoresearch West Grove PA, USA), diluted 1:1000 for 40 min at room temperature, washed in PBS, and stained with 2 mM Hoechst 33258 (Molecular Probes), slides were rinsed in PBS and mounted in Prolong antifade (Invitrogen, Barcelona, Spain). Images were photographed using a Zeiss Axiovert 200M microscope (Barcelona, Spain). All microphotographs were obtained with identical parameters for intensity, pinhole aperture, etc.

Apoptosis was identified using TUNEL "In situ Cell Death Detection Kit" (Roche, Burgess Hill, UK), which allows detection and quantification of apoptosis at the single-cell level, based on labeling of DNA strand breaks. TUNEL staining was performed on paraffin-embedded tissues according to the manufacturer´s instructions.

Fibroblasts and tubular epithelial cells in cover slips were fixed with 4% paraformaldehyde (Sigma-Aldrich), washed with PBS, permeabilized with 0.1% Triton X-100, blocked 30 min with 2% bovine serum albumin in PBS, treated with PBS–0.05% Tween 20 for 10 min, and incubated during 2 h with primary antibodies: Rat anti-cardiotrophin-1 (RD System; dilution 1:100), rabbit anti-gp130 (Cell Signaling; dilution 1:100), rabbit anti-LIFR (Santa Cruz Biotechnology; dilution 1:100), mouse anti-e-cadherin (Pharmingen, BD, Madrid, Spain; dilution 1:100), mouse anti-pan-cytokeratin (Santa Cruz Biotechnology; dilution 1:50) or mouse anti-α-SMA (Sigma-Aldrich; dilution 1:100). Later, cells were incubated 30 min with goat anti-mouse or anti-rabbit CY3 or donkey anti-rat CY3 (Jackson Immunoresearch) in PBS in a dark chamber. Nuclei staining was performed by 5 min incubation with 2 mM Hoechst 33258 (Molecular Probes) in a dark chamber. Cover slips were mounted on slides using Prolong Antifade (Invitrogen). Images were obtained as previously described. All experiments were performed by triplicate.

Statistical analysis

Data are expressed as mean ± standard error of the mean (SEM). The Kolmogorov–Smirnov test was used to assess the normality of the data distribution. Comparison of means was performed by one way analysis of variance (ANOVA) and Dunnett post hot test. Statistical differences between two groups were assessed by the Student "t" test. Statistical analysis was performed using GraphPad Prism version 5.00 for Windows (GraphPad Software, San Diego, California, USA, www.graphpad.com). A "p" value lower than 0.05 was considered statistically significant. The data and statistical

analysis comply with the recommendations on experimental design and analysis in pharmacology (Curtis et al., 2015).

ACKNOWLEDGEMENTS

This work was supported by grants from Instituto de Salud Carlos III (Ministry of Economy and Competitiveness, PI12/00959, PI15/01055, Kidney Research Network REDINREN RD012/0021/0032 and RD016/0009/0025, co-funded by FEDER), Junta de Castilla y León (Ministry of Health, BIO/SA87/13) and Fundación Mutua Madrileña (IX Call for Grants and Aids for Medical Research).

Conflict of interest statement: the authors declare that no conflict of interest exists

REFERENCES

1. Quiros Y, Ferreira L, Sancho-Martinez SM, Gonzalez-Buitrago JM, Lopez-Novoa JM, Lopez-Hernandez FJ. Sub-nephrotoxic doses of gentamicin predispose animals to developing acute kidney injury and to excrete ganglioside M2 activator protein. *Kidney Int.* 2010;78(10):1006-1015.
2. Lopez-Novoa JM, Rodriguez-Pena AB, Ortiz A, Martinez-Salgado C, Lopez Hernandez FJ. Etiopathology of chronic tubular, glomerular and renovascular nephropathies: clinical implications. *Journal of translational medicine.* 2011;9:13.
3. Zeisberg M, Neilson EG. Mechanisms of tubulointerstitial fibrosis. *Journal of the American Society of Nephrology : JASN.* 2010;21(11):1819-1834.
4. Grande MT, Lopez-Novoa JM. Fibroblast activation and myofibroblast generation in obstructive nephropathy. *Nat Rev Nephrol.* 2009;5(6):319-328.
5. Boor P, Ostendorf T, Floege J. Renal fibrosis: novel insights into mechanisms and therapeutic targets. *Nature reviews Nephrology.* 2010;6(11):643-656.
6. Nogueira A, Pires MJ, Oliveira PA. Pathophysiological Mechanisms of Renal Fibrosis: A Review of Animal Models and Therapeutic Strategies. *In Vivo.* 2017;31(1):1-22.
7. Pennica D, Wood WI, Chien KR. Cardiotrophin-1: a multifunctional cytokine that signals via LIF receptor-gp 130 dependent pathways. *Cytokine & growth factor reviews.* 1996;7(1):81-91.
8. Pennica D, King KL, Shaw KJ, et al. Expression cloning of cardiotrophin 1, a cytokine that induces cardiac myocyte hypertrophy. *Proceedings of the National Academy of Sciences of the United States of America.* 1995;92(4):1142-1146.

9. Liao Z, Brar BK, Cai Q, et al. Cardiotrophin-1 (CT-1) can protect the adult heart from injury when added both prior to ischaemia and at reperfusion. *Cardiovascular research.* 2002;53(4):902-910.
10. Railson J, Lawrence K, Stephanou A, Brar B, Pennica D, Latchman D. Cardiotrophin-1 reduces stress-induced heat shock protein production in cardiac myocytes. *Cytokine.* 2000;12(11):1741-1744.
11. Oppenheim RW, Wiese S, Prevette D, et al. Cardiotrophin-1, a muscle-derived cytokine, is required for the survival of subpopulations of developing motoneurons. *The Journal of neuroscience : the official journal of the Society for Neuroscience.* 2001;21(4):1283-1291.
12. Peng H, Sola A, Moore J, Wen T. Caspase inhibition by cardiotrophin-1 prevents neuronal death in vivo and in vitro. *Journal of neuroscience research.* 2010;88(5):1041-1051.
13. Garcia-Cenador MB, Lorenzo-Gomez MF, Herrero-Payo JJ, et al. Cardiotrophin-1 administration protects from ischemia-reperfusion renal injury and inflammation. *Transplantation.* 2013;96(12):1034-1042.
14. Bustos M, Beraza N, Lasarte JJ, et al. Protection against liver damage by cardiotrophin-1: a hepatocyte survival factor up-regulated in the regenerating liver in rats. *Gastroenterology.* 2003;125(1):192-201.
15. Aguilar-Melero P, Luque A, Machuca MM, et al. Cardiotrophin-1 reduces ischemia/reperfusion injury during liver transplant. *The Journal of surgical research.* 2013;181(2):e83-91.
16. Iniguez M, Berasain C, Martinez-Anso E, et al. Cardiotrophin-1 defends the liver against ischemia-reperfusion injury and mediates the protective effect of ischemic preconditioning. *The Journal of experimental medicine.* 2006;203(13):2809-2815.
17. Ho DW, Yang ZF, Lau CK, et al. Therapeutic potential of cardiotrophin 1 in fulminant hepatic failure: dual roles in antiapoptosis and cell repair. *Arch Surg.* 2006;141(11):1077-1084; discussion 1084.
18. Tunon MJ, San Miguel B, Crespo I, et al. Melatonin attenuates apoptotic liver damage in fulminant hepatic failure induced by the rabbit hemorrhagic disease virus. *Journal of pineal research.* 2011;50(1):38-45.
19. Benigni F, Sacco S, Pennica D, Ghezzi P. Cardiotrophin-1 inhibits tumor necrosis factor production in the heart and serum of lipopolysaccharide-treated mice and in vitro in mouse blood cells. *The American journal of pathology.* 1996;149(6):1847-1850.
20. Quiros Y, Sanchez-Gonzalez PD, Lopez-Hernandez FJ, Morales AI, Lopez-Novoa JM. Cardiotrophin-1 administration prevents the renal toxicity of iodinated contrast media in rats. *Toxicological sciences : an official journal of the Society of Toxicology.* 2013;132(2):493-501.
21. Quiros Y, Blanco-Gozalo V, Sanchez-Gallego JI, et al. Cardiotrophin-1 therapy prevents gentamicin-induced nephrotoxicity in rats. *Pharmacological research.* 2016;107:137-146.
22. Border WA, Noble NA. TGF-beta in kidney fibrosis: a target for gene therapy. *Kidney international.* 1997;51(5):1388-1396.
23. Ucero AC, Benito-Martin A, Izquierdo MC, et al. Unilateral ureteral obstruction: beyond obstruction. *Int Urol Nephrol.* 2014;46(4):765-776.
24. Ardura JA, Berruguete R, Ramila D, Alvarez-Arroyo MV, Esbrit P. Parathyroid hormone-related protein interacts with vascular endothelial growth factor to promote fibrogenesis in the obstructed mouse kidney. *American journal of physiology Renal physiology.* 2008;295(2):F415-425.
25. Sancho-Martinez SM, Lopez-Novoa JM, Lopez-Hernandez FJ. Pathophysiological role of different tubular epithelial cell death modes in acute kidney injury. *Clinical kidney journal.* 2015;8(5):548-559.

26. Misaki T, Yamamoto T, Suzuki S, et al. Decrease in tumor necrosis factor-alpha receptor-associated death domain results from ubiquitin-dependent degradation in obstructive renal injury in rats. *The American journal of pathology.* 2009;175(1):74-83.
27. Strutz F, Zeisberg M. Renal fibroblasts and myofibroblasts in chronic kidney disease. *Journal of the American Society of Nephrology : JASN.* 2006;17(11):2992-2998.
28. Yoo KH, Thornhill BA, Forbes MS, et al. Osteopontin regulates renal apoptosis and interstitial fibrosis in neonatal chronic unilateral ureteral obstruction. *Kidney international.* 2006;70(10):1735-1741.
29. Morrissey JJ, Klahr S. Differential effects of ACE and AT1 receptor inhibition on chemoattractant and adhesion molecule synthesis. *The American journal of physiology.* 1998;274(3 Pt 2):F580-586.
30. Lee J, Bae EH, Ma SK, Kim SW. Altered Nitric Oxide System in Cardiovascular and Renal Diseases. *Chonnam medical journal.* 2016;52(2):81-90.
31. Honma S, Shinohara M, Takahashi N, et al. Effect of cyclooxygenase (COX)-2 inhibition on mouse renal interstitial fibrosis. *European journal of pharmacology.* 2014;740:578-583.
32. Morrissey J, Klahr S. Transcription factor NF-kappaB regulation of renal fibrosis during ureteral obstruction. *Seminars in nephrology.* 1998;18(6):603-611.
33. Morrissey JJ, Klahr S. Rapid communication. Enalapril decreases nuclear factor kappa B activation in the kidney with ureteral obstruction. *Kidney international.* 1997;52(4):926-933.
34. Grande MT, Perez-Barriocanal F, Lopez-Novoa JM. Role of inflammation in tubulo-interstitial damage associated to obstructive nephropathy. *J Inflamm (Lond).* 2010;7:19.
35. Musial A, Eissa NT. Inducible nitric-oxide synthase is regulated by the proteasome degradation pathway. *The Journal of biological chemistry.* 2001;276(26):24268-24273.
36. Tashiro K, Tamada S, Kuwabara N, et al. Attenuation of renal fibrosis by proteasome inhibition in rat obstructive nephropathy: possible role of nuclear factor kappaB. *International journal of molecular medicine.* 2003;12(4):587-592.
37. Chevalier RL, Forbes MS, Thornhill BA. Ureteral obstruction as a model of renal interstitial fibrosis and obstructive nephropathy. *Kidney international.* 2009;75(11):1145-1152.
38. Gamella-Pozuelo L, Fuentes-Calvo I, Gomez-Marcos MA, et al. Plasma Cardiotrophin-1 as a Marker of Hypertension and Diabetes-Induced Target Organ Damage and Cardiovascular Risk. *Medicine.* 2015;94(30):e1218.
39. Lopez-Yoldi M, Moreno-Aliaga MJ, Bustos M. Cardiotrophin-1: A multifaceted cytokine. *Cytokine & growth factor reviews.* 2015;26(5):523-532.
40. Bhattacharya S, Ray RM, Johnson LR. STAT3-mediated transcription of Bcl-2, Mcl-1 and c-IAP2 prevents apoptosis in polyamine-depleted cells. *The Biochemical journal.* 2005;392(Pt 2):335-344.
41. Catlett-Falcone R, Landowski TH, Oshiro MM, et al. Constitutive activation of Stat3 signaling confers resistance to apoptosis in human U266 myeloma cells. *Immunity.* 1999;10(1):105-115.
42. Koike K, Ueda S, Yamagishi S, et al. Protective role of JAK/STAT signaling against renal fibrosis in mice with unilateral ureteral obstruction. *Clin Immunol.* 2014;150(1):78-87.
43. Kawada N, Moriyama T, Ando A, et al. Increased oxidative stress in mouse kidneys with unilateral ureteral obstruction. *Kidney international.* 1999;56(3):1004-1013.
44. Klahr S. Urinary tract obstruction. *Seminars in nephrology.* 2001;21(2):133-145.
45. Schaier M, Jocks T, Grone HJ, Ritz E, Wagner J. Retinoid agonist isotretinoin ameliorates obstructive renal injury. *The Journal of urology.* 2003;170(4 Pt 1):1398-1402.
46. Sauer H, Neukirchen W, Rahimi G, Grunheck F, Hescheler J, Wartenberg M. Involvement of reactive oxygen species in cardiotrophin-1-induced proliferation of cardiomyocytes differentiated from murine embryonic stem cells. *Experimental cell research.* 2004;294(2):313-324.

47. Hishinuma S, Funamoto M, Fujio Y, Kunisada K, Yamauchi-Takihara K. Hypoxic stress induces cardiotrophin-1 expression in cardiac myocytes. *Biochemical and biophysical research communications.* 1999;264(2):436-440.
48. Meldrum KK, Metcalfe P, Leslie JA, Misseri R, Hile KL, Meldrum DR. TNF-alpha neutralization decreases nuclear factor-kappaB activation and apoptosis during renal obstruction. *The Journal of surgical research.* 2006;131(2):182-188.
49. Sanz AB, Sanchez-Nino MD, Ramos AM, et al. NF-kappaB in renal inflammation. *Journal of the American Society of Nephrology : JASN.* 2010;21(8):1254-1262.
50. Nam NH. Naturally occurring NF-kappaB inhibitors. *Mini reviews in medicinal chemistry.* 2006;6(8):945-951.
51. Blackwell TS, Christman JW. The role of nuclear factor-kappa B in cytokine gene regulation. *American journal of respiratory cell and molecular biology.* 1997;17(1):3-9.
52. Lopez N, Diez J, Fortuno MA. Characterization of the protective effects of cardiotrophin-1 against non-ischemic death stimuli in adult cardiomyocytes. *Cytokine.* 2005;30(5):282-292.
53. Negoro S, Kunisada K, Fujio Y, et al. Activation of signal transducer and activator of transcription 3 protects cardiomyocytes from hypoxia/reoxygenation-induced oxidative stress through the upregulation of manganese superoxide dismutase. *Circulation.* 2001;104(9):979-981.
54. Lopez-Andres N, Rousseau A, Akhtar R, et al. Cardiotrophin 1 is involved in cardiac, vascular, and renal fibrosis and dysfunction. *Hypertension.* 2012;60(2):563-573.
55. Garcia-Cenador MB, Lopez-Novoa JM, Diez J, Garcia-Criado FJ. Effects and mechanism of organ protection by cardiotrophin-1. *Current medicinal chemistry.* 2013;20(2):246-256.
56. Rodriguez-Pena AB, Grande MT, Eleno N, et al. Activation of Erk1/2 and Akt following unilateral ureteral obstruction. *Kidney international.* 2008;74(2):196-209.
57. Muller GA, Markovic-Lipkovski J, Frank J, Rodemann HP. The role of interstitial cells in the progression of renal diseases. *Journal of the American Society of Nephrology : JASN.* 1992;2(10 Suppl):S198-205.
58. Nagatoya K, Moriyama T, Kawada N, et al. Y-27632 prevents tubulointerstitial fibrosis in mouse kidneys with unilateral ureteral obstruction. *Kidney international.* 2002;61(5):1684-1695.
59. Munoz-Felix JM, Lopez-Novoa JM, Martinez-Salgado C. Heterozygous disruption of activin receptor-like kinase 1 is associated with increased renal fibrosis in a mouse model of obstructive nephropathy. *Kidney international.* 2014;85(2):319-332.
60. Sharpe CC, Dockrell ME, Noor MI, Monia BP, Hendry BM. Role of Ras isoforms in the stimulated proliferation of human renal fibroblasts in primary culture. *Journal of the American Society of Nephrology : JASN.* 2000;11(9):1600-1606.
61. Sharpe CC, Dockrell ME. Primary culture of human renal proximal tubule epithelial cells and interstitial fibroblasts. *Methods Mol Biol.* 2012;806:175-185.

FIGURE LEGENDS

Figure 1. Effects of cardiotrophin-1 (CT-1) deficiency in interstitial fibrosis and extracellular matrix proteins expression after 15 days of unilateral ureteral obstruction. Representative images of Sirius red and quantification of stained area (A) and Masson's trichrome staining (B) in obstructed and contralateral, non obstructed kidneys from WT and CT-$1^{-/-}$ mice. (C) Collagen I mRNA levels in obstructed kidneys from WT and CT-$1^{-/-}$ mice. (D) Total collagen synthesis in obstructed kidneys from WT and CT-$1^{-/-}$ mice. (E) Western blot analysis of fibronectin, connective tissue growth factor (CTGF) and collagen I expression in obstructed kidneys from WT and CT-$1^{-/-}$ mice (WT n=6, CT-$1^{-/-}$ n=6). Bar= 10 µm. * $p<0.05$, † $p<0.01$. AU: arbitrary units.

Figure 2. Effects of cardiotrophin-1 (CT-1) deficiency in tubular damage, apoptosis and myofibroblasts abundance after 3 days of unilateral ureteral obstruction. (A) Representative images of renal cortex sections in obstructed kidneys from WT and CT-$1^{-/-}$ mice stained with hematoxylin-eosin and quantification of injury score (n=6). Arrowheads mark cellular debris, short arrows mark hyaline deposits, long arrows mark hyaline accumulation and stars mark tubular dilatation. (B) Western blot analysis of cleaved caspase-3 expression in obstructed kidneys from WT and CT-$1^{-/-}$ mice. (C) Representative images of cleaved caspase-3 immunohistochemistry on renal cortex in obstructed kidneys from WT and CT-$1^{-/-}$ mice. (D) Representative images of TUNEL staining on renal cortex and corticomedular area in obstructed kidneys from WT and CT-$1^{-/-}$ mice visualized by fluorescent microscopy. (E) Western blot analysis of phospho-STAT3 expression in obstructed kidneys from WT and CT-$1^{-/-}$ mice. (F) Western blot analysis of α-smooth muscle actin (α-SMA) expression in obstructed kidneys from WT and CT-$1^{-/-}$ mice. (G) Representative images of α-SMA and vimentin immunohistochemistry on renal cortex in obstructed kidneys from WT and CT-$1^{-/-}$ mice (WT n=6, CT-$1^{-/-}$ n=6). Bar= 10 µm. * $p<0.05$, † $p<0.01$. AU: arbitrary units.

Figure 3. Effects of cardiotrophin-1 (CT-1) deficiency in the inflammatory response after 3 days of unilateral ureteral obstruction. (A) Quantification of Cd68 mRNA levels in obstructed kidneys from WT and CT-$1^{-/-}$ mice. Western blot analysis of intercellular adhesion molecule 1 (ICAM-1), cyclooxygenase-2 (COX-2) (B), inducible nitric oxide synthase (iNOs) (C) pp65 and IκB-α (E) in obstructed kidneys from WT and CT-$1^{-/-}$ mice. (D) Representative images of iNOs immunohistochemistry in renal cortex in obstructed kidneys from WT and CT-$1^{-/-}$ mice (WT n=6, CT-$1^{-/-}$ n=6). Bar= 10 µm. * $p<0.05$, † $p<0.01$.

Figure 4. Effects of cardiotrophin-1 (CT-1) administration in interstitial fibrosis and extracellular matrix proteins expression after 15 days of unilateral ureteral obstruction in CT-$1^{-/-}$ mice. (A) Representative images of Masson's trichrome and Sirius red staining in obstructed kidneys from CT-$1^{-/-}$, CT-1 100 µg kg^{-1} and 400 µg kg^{-1} treated mice and Image-Pro Plus quantification of the Sirius red stained area. Bar= 10 µm. (B) Fibronectin and collagen I mRNA levels in obstructed kidneys from CT-$1^{-/-}$, CT-1 100 µg kg^{-1} and 400 µg kg^{-1} treated mice. Western blot analysis of fibronectin, collagen I (C), α-smooth muscle actin (α-SMA) and proliferating cell nuclear antigen (PCNA) expression (D) in obstructed kidneys from CT-$1^{-/-}$, CT-1 100 µg kg^{-1} and 400 µg kg^{-1} treated mice. (E) Representative images of α-SMA immunofluorescence in obstructed kidneys from CT-$1^{-/-}$, CT-1 100 µg kg^{-1} and 400 µg kg^{-1} treated mice. Bar= 20 µm. (F) Representative images of vimentin immunohistochemistry on renal cortex in obstructed kidneys from CT-$1^{-/-}$, CT-1 100 µg kg^{-1} and 400 µg kg^{-1} treated mice. Bar= 10 µm. (CT-$1^{-/-}$, n=6; CT-1 100 µg kg^{-1}, n=5; CT-1 400 µg kg^{-1}, n=5). * $p<0.05$, † $p<0.01$. AU: arbitrary units.

Figure 5. Effects of cardiotrophin-1 (CT-1) administration in tubular injury, cell apoptosis and myofibroblasts abundance after 3 days of unilateral ureteral obstruction in CT-$1^{-/-}$ mice. (A) Representative images of renal cortex sections stained with hematoxylin-eosin in non obstructed and obstructed kidneys from CT-$1^{-/-}$, CT-1 100 µg kg^{-1} and 400 µg kg^{-1} treated mice and quantification

of injury score (B). (C) Western blot analysis of cleaved caspase-3 protein expression in obstructed kidneys from CT-$1^{-/-}$, CT-1 100 μg kg^{-1} and 400 μg kg^{-1} treated mice. (D) Representative images of cleaved caspase-3 immunohistochemistry on renal cortex in obstructed kidneys from CT-$1^{-/-}$, CT-1 100 μg kg^{-1} and 400 μg kg^{-1} treated mice. (E) Representative images of TUNEL staining on renal cortex and corticomedullary area in obstructed kidneys from CT-$1^{-/-}$, CT-1 100 μg kg^{-1} and 400 μg kg^{-1} treated mice visualized by fluorescent microscopy. Representative images of vimentin (F) and α-smooth muscle actin (α-SMA) (G) immunohistochemistry on renal cortex in obstructed kidneys from CT-$1^{-/-}$, CT-1 100 μg kg^{-1} and 400 μg kg^{-1} treated mice. (H) Western blot analysis of α-SMA expression in obstructed kidneys from CT-$1^{-/-}$ and CT-1 400 μg kg^{-1} treated mice (CT-$1^{-/-}$, n=6; CT-1 100 μg kg^{-1}, n=5; CT-1 400 μg kg^{-1}, n=6). Bar= 10 μm. * $p<0.05$, † $p<0.01$. AU: arbitrary units.

Figure 6. Effects of cardiotrophin-1 (CT-1) administration in the inflammatory response after 3 days of unilateral ureteral obstruction in CT-$1^{-/-}$ mice. (A) Cd68 and interleukin-1β (IL-1β) mRNA levels in obstructed kidneys from CT-$1^{-/-}$, CT-1 100 μg kg^{-1} and 400 μg kg^{-1} treated mice. (B) Western blot analysis of vascular cell adhesion molecule 1 (VCAM-1), IκB-α and cyclooxygenase-2 (COX-2) expression in obstructed kidneys from CT-$1^{-/-}$, CT-1 100 μg kg^{-1} and 400 μg kg^{-1}treated mice. (C) Representative images of inducible nitric oxide synthase (iNOs) immunohistochemistry on renal cortex in obstructed kidneys from CT-$1^{-/-}$, CT-1 100 μg kg^{-1} and 400 μg kg^{-1} treated mice (CT-$1^{-/-}$, n=6; CT-1 100 μg kg^{-1}, n=5; CT-1 400 μg kg^{-1}, n=6). Bar= 10 μm. * $p<0.05$, † $p<0.01$.

Figure 7. Effects of cardiotrophin-1 (CT-1) administration in interstitial fibrosis and extracellular matrix proteins expression after 15 days of unilateral ureteral obstruction in WT mice. (A) Representative images of Masson's trichrome and Sirius red staining in obstructed kidneys from WT, CT-1 100 μg kg^{-1} and 400 μg kg^{-1} treated mice and Image-Pro Plus quantification of the Sirius red stained area. (B) Western blot analysis of fibronectin, connective tissue growth factor (CTGF) and collagen I expressions in obstructed kidneys from WT, CT-1 100 μg kg^{-1} and 400 μg kg^{-1} treated mice

(WT, n=6; CT-1 100 μg kg^{-1}, n=5; CT-1 400 μg kg^{-1}, n=5). Bar= 10 μm. * $p<0.05$, † $p<0.01$. AU: arbitrary units.

Figure 8. Effects of cardiotrophin-1 (CT-1) administration in tubular injury, cell apoptosis and myofibroblasts abundance after 3 days of unilateral ureteral obstruction in WT mice. (A) Representative images of renal cortex sections stained with hematoxylin-eosin in non obstructed and obstructed kidneys from WT, CT-1 100 μg kg^{-1} and 400 μg kg^{-1} treated mice, and quantification of injury score (B). (C) Western blot analysis of cleaved caspase-3 expression in obstructed kidneys from WT, CT-1 100 μg kg^{-1} and 400 μg kg^{-1} treated mice. (D) Representative images of cleaved caspase-3 immunohistochemistry on renal cortex in obstructed kidneys from WT, CT-1 100 μg kg^{-1} and 400 μg kg^{-1} treated mice. (E) Representative images of TUNEL staining on renal cortex and corticomedular area in obstructed kidneys from WT, CT-1 100 μg kg^{-1} and 400 μg kg^{-1}treated mice, visualized by fluorescent microscopy. (F) Western blot analysis of α-smooth muscle actin (α-SMA) and proliferation cellular nuclear antigen (PCNA) expression in obstructed kidneys from WT, CT-1 100 μg kg^{-1} and 400 μg kg^{-1} treated mice. (G) Representative images of vimentin immunohistochemistry on renal cortex in obstructed kidneys from WT, CT-1 100 μg kg^{-1} and 400 μg kg^{-1} treated mice (WT, n=6; CT-1 100 μg kg^{-1}, n=5; CT-1 400 μg kg^{-1}, n=6). Bar= 10 μm. * $p<0.05$, † $p<0.01$. AU: arbitrary units

Figure 9. Effects of cardiotrophin-1 (CT-1) administration in the inflammatory response after 3 days of unilateral ureteral obstruction in WT mice. (A) Cd68 and interleukin-1β (IL-1β) mRNA levels in obstructed kidneys from WT, CT-1 100 μg kg^{-1} and 400 μg kg^{-1} treated mice. Western blot analysis of intercellular adhesion molecule 1 (ICAM-1), cyclooxygenase-2 (COX-2), pp65 and IκB-α expression (B) in obstructed kidneys from WT, CT-1 100 μg kg^{-1} and 400 μg kg^{-1} treated mice. (C) Representative images of inducible nitric oxide synthase (iNOs) immunohistochemistry on renal cortex in obstructed

kidneys from WT, CT-1 100 µg kg^{-1} and 400 µg kg^{-1} treated mice. WT, n=6; CT-1 100 µg kg^{-1}, n=5; CT-1 400 µg kg^{-1}, n=6). Bar= 10 µm. * p<0.05, † p<0.01.

Figure 10. Effect of unilateral ureteral obstruction in cardiotrophin-1 (CT-1) expression and effects of CT-1 in tubular epithelial cells and renal myofibroblasts *in vitro*. (A) Quantification of CT-1 mRNA levels in non obstructed (n=6) and obstructed (n=6) kidneys from WT mice. (B) Representative images of CT-1 immunohistochemistry in non obstructed and obstructed kidneys from WT mice. Bar= 10 µm. Representative Western blot images of CT-1 expression in WT and CT-$1^{-/-}$ renal myofibroblasts (C) and tubular epithelial cells (E). (D) CT-1 immunofluorescence in WT and CT-$1^{-/-}$ renal myofibroblasts. Bar= 20 µm. Glycoprotein 130 (gp130) and leukemia inhibitory factor receptor (LIFR) immunofluorescence in WT renal myofibroblasts (F) and tubular epithelial cells (G). Bar= 10 µm. Representative Western blot images of phospho-STAT3 expression in WT renal myofibroblasts (H) and phospho-STAT3 expression in tubular epithelial cells (I). Western blot analysis of collagen I, fibronectin (J), pp65 and IκBα (K) protein expression in WT and CT-$1^{-/-}$ renal myofibroblasts. * p<0.05, † p<0.01. FCS: fetal calf serum.

Supplementary figures:

Suppl. Figure 1. (A) Representative images of renal cortex sections stained with hematoxylin-eosin from obstructed and non obstructed kidneys from WT and CT-$1^{-/-}$ mice after 15 days of unilateral ureteral obstruction. Bar=10 µm. (B) Representative micrographs of renal cortex sections stained with hematoxylin-eosin from obstructed and non obstructed kidneys from WT and CT-$1^{-/-}$ mice after 15 days of unilateral ureteral obstruction. Bar= 100 µm (non obstructed CT-$1^{+/+}$, n=6; obstructed CT-$1^{+/+}$, n=6; non obstructed CT-$1^{-/-}$, n=6; obstructed CT-$1^{-/-}$, n=6). Long arrows mark tubular dilatation, short arrows mark tubular atrophy and arrowheads mark hypercellularity.

Suppl. Figure 2. Representative micrographs of Sirius red (A) and Masson's trichrome staining (B) in obstructed and non obstructed kidneys from WT and CT-$1^{-/-}$ mice after 15 days of unilateral ureteral obstruction (non obstructed CT-$1^{+/+}$, n=6; obstructed CT-$1^{+/+}$, n=6; non obstructed CT-$1^{-/-}$, n=6; obstructed CT-$1^{-/-}$, n=6). Bar= 100 µm. (C) Representative images of renal cortex sections stained with hematoxylin-eosin of non obstructed kidneys from WT and CT-$1^{-/-}$ mice after 3 days of unilateral ureteral obstruction. (WT n=6, CT-$1^{-/-}$ n=6). Bar= 10 µm.

Suppl. Figure 3. (A) Representative micrographs of renal cortex sections in obstructed kidneys from WT and CT-$1^{-/-}$ mice stained with hematoxylin-eosin after 3 days of unilateral ureteral obstruction (WT n=6, CT-$1^{-/-}$ n=6). (B) Representative micrographs of Masson's trichrome and Sirius red staining in obstructed kidneys from CT-$1^{-/-}$, CT-1 100 µg kg^{-1} and 400 µg kg^{-1} treated mice after 15 days of unilateral ureteral obstruction (CT-$1^{-/-}$, n=6; CT-1 100 µg kg^{-1}, n=5; CT-1 400 µg kg^{-1}, n=5). (C) Representative images of renal cortex sections stained with hematoxylin-eosin in non obstructed and obstructed kidneys from CT-$1^{-/-}$, CT-1 100 µg kg^{-1} and 400 µg kg^{-1} treated mice after 3 days of unilateral ureteral obstruction (CT-$1^{-/-}$, n=6; CT-1 100 µg kg^{-1}, n=5; CT-1 400 µg kg^{-1}, n=6). Bar= 100 µm

Suppl. Figure 4. (A) Representative micrographs of Masson's trichrome and Sirius red staining in obstructed kidneys from WT, CT-1 100 µg kg^{-1} and 400 µg kg^{-1} treated mice after 15 days of unilateral ureteral obstruction (WT, n=6; CT-1 100 µg kg^{-1}, n=5; CT-1 400 µg kg^{-1}, n=5). (B) Representative micrographs of renal cortex sections stained with hematoxylin-eosin in non obstructed and obstructed kidneys from WT, CT-1 100 µg kg^{-1} and 400 µg kg^{-1} treated mice after 3 days of unilateral ureteral obstruction (WT, n=6; CT-1 100 µg kg^{-1}, n=5; CT-1 400 µg kg^{-1}, n=6). Bar= 100 µm**.** (C) Representative images of α-smooth muscle actin (α-SMA) immunohistochemistry on renal cortex in obstructed kidneys from WT, CT-1 100 µg kg^{-1} and 400 µg kg^{-1} treated mice (WT, n=6; CT-1 100 µg kg^{-}

^{1}, n=5; CT-1 400 µg kg^{-1}, n=6). Bar= 10 µm. (D) Representative Western blot images of cardiotrophin-1 (CT-1) expression in healthy kidneys from WT and CT-1$^{-/-}$ mice (WT n=6, CT-1 $^{-/-}$ n=6).

Suppl. Figure 5. (A) α-smooth muscle actin (α-SMA) immunofluorescence in WT and CT-1$^{-/-}$ renal myofibroblasts. Bar= 50 µm. (B) e-cadherin and pan-cytokeratin immunofluorescence in tubular epithelial cells. Bar= 10 µm

Figure 1

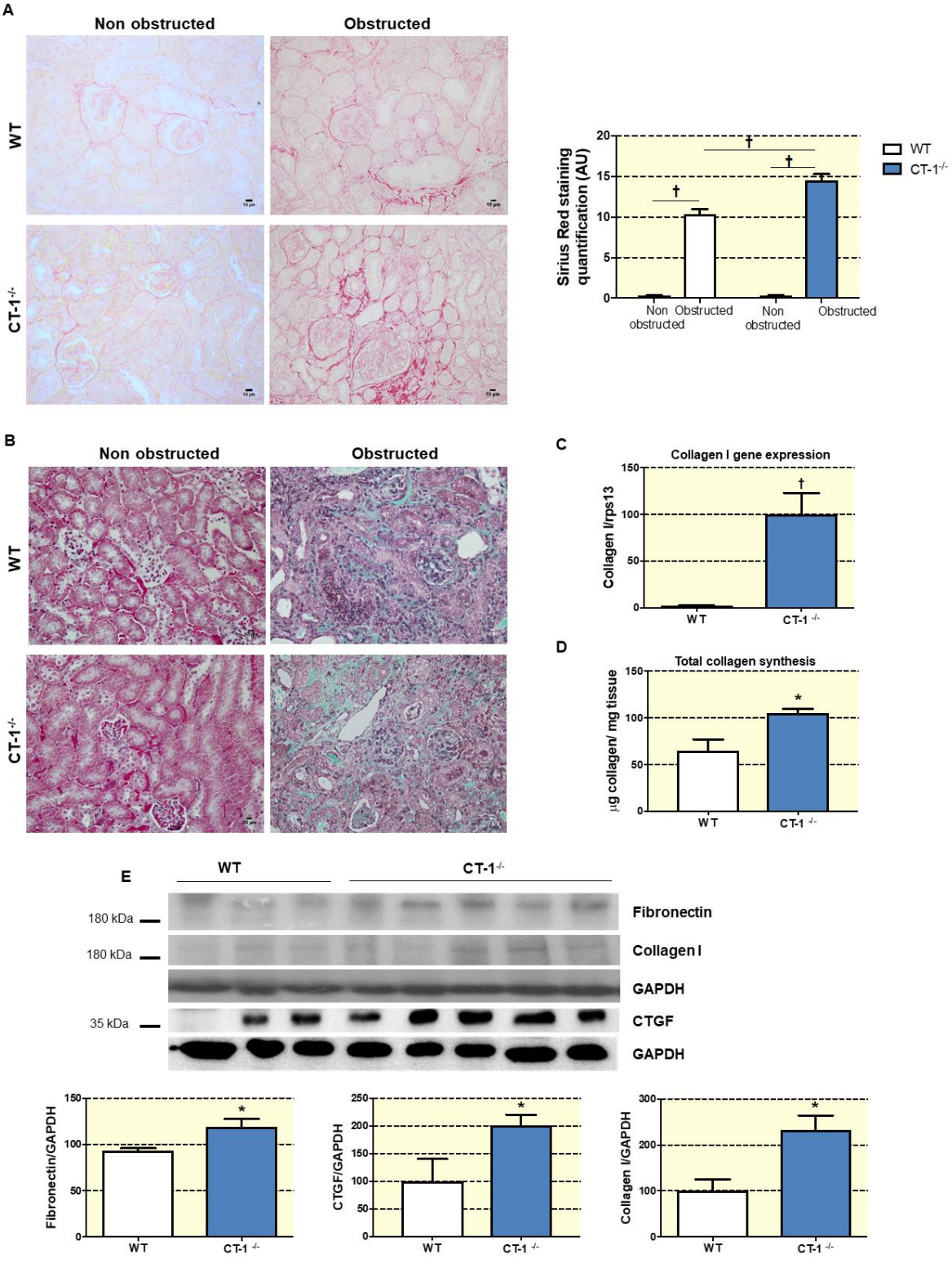

Figure 2

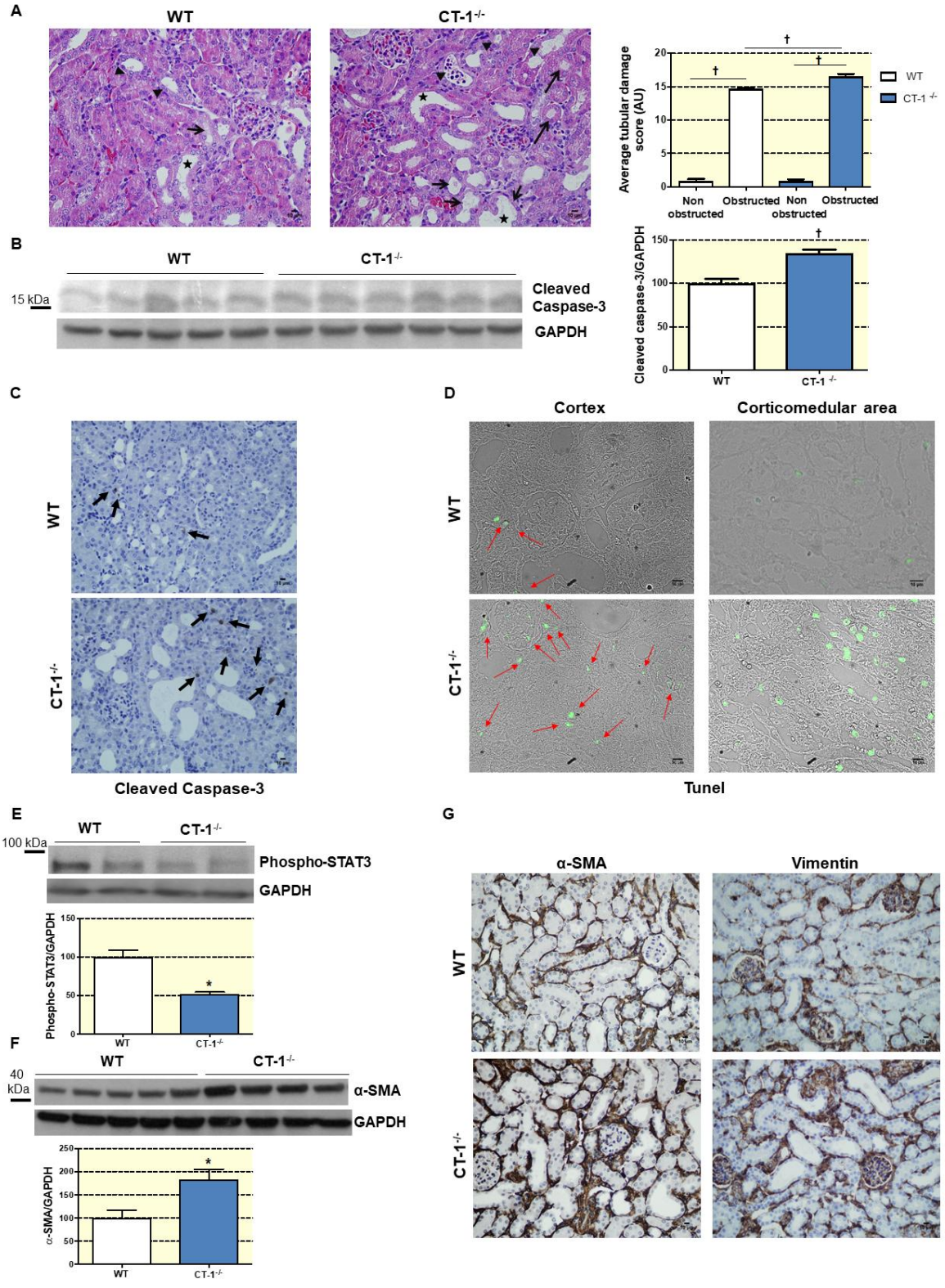

Figure 3

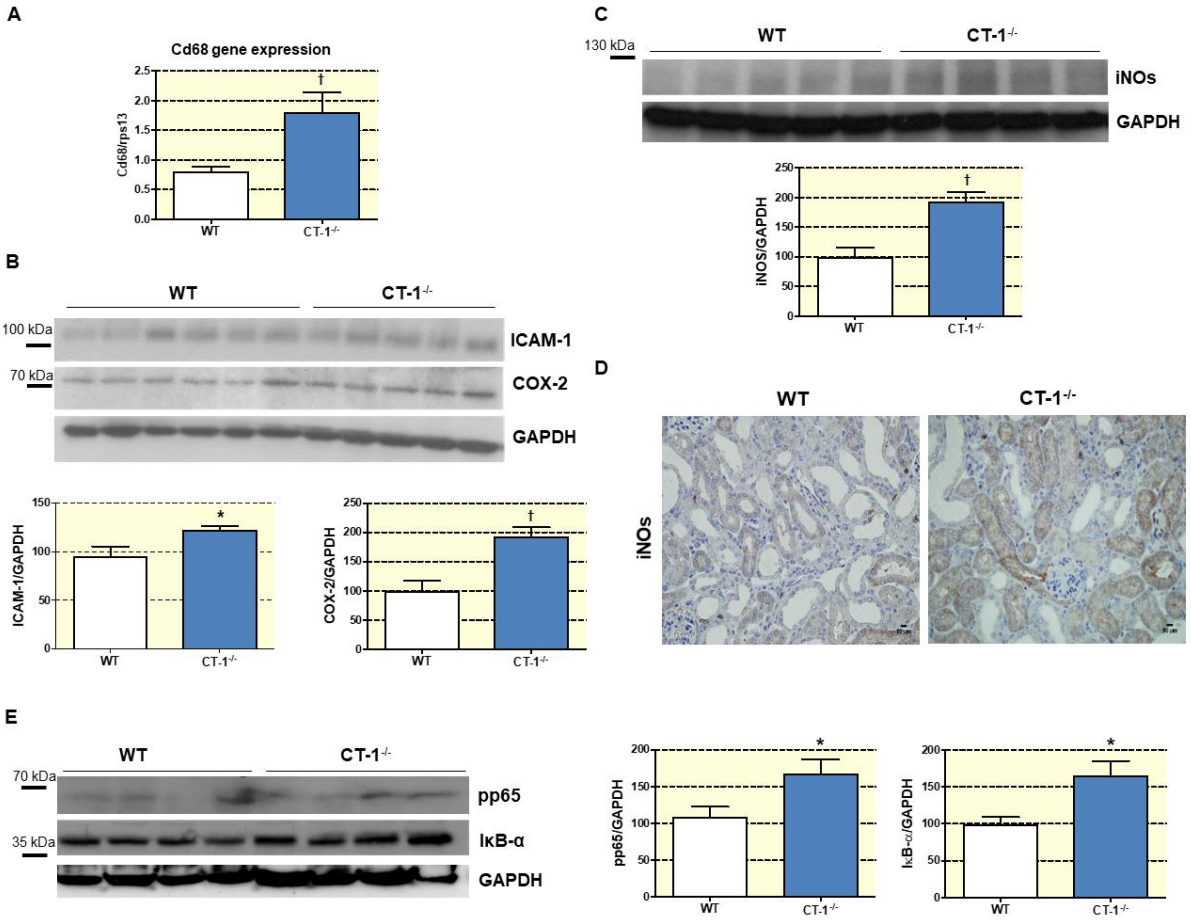

Figure 4

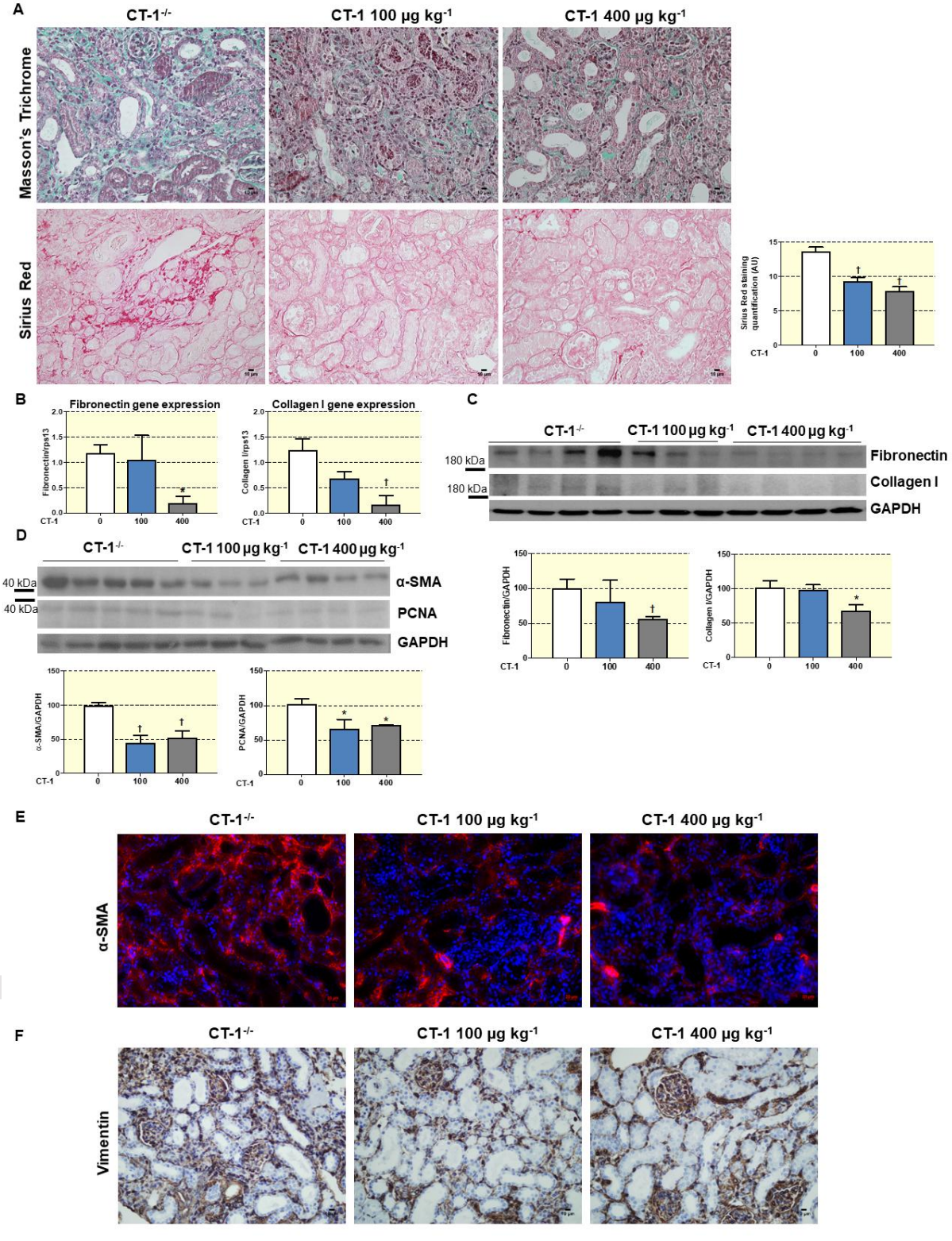

Figure 5

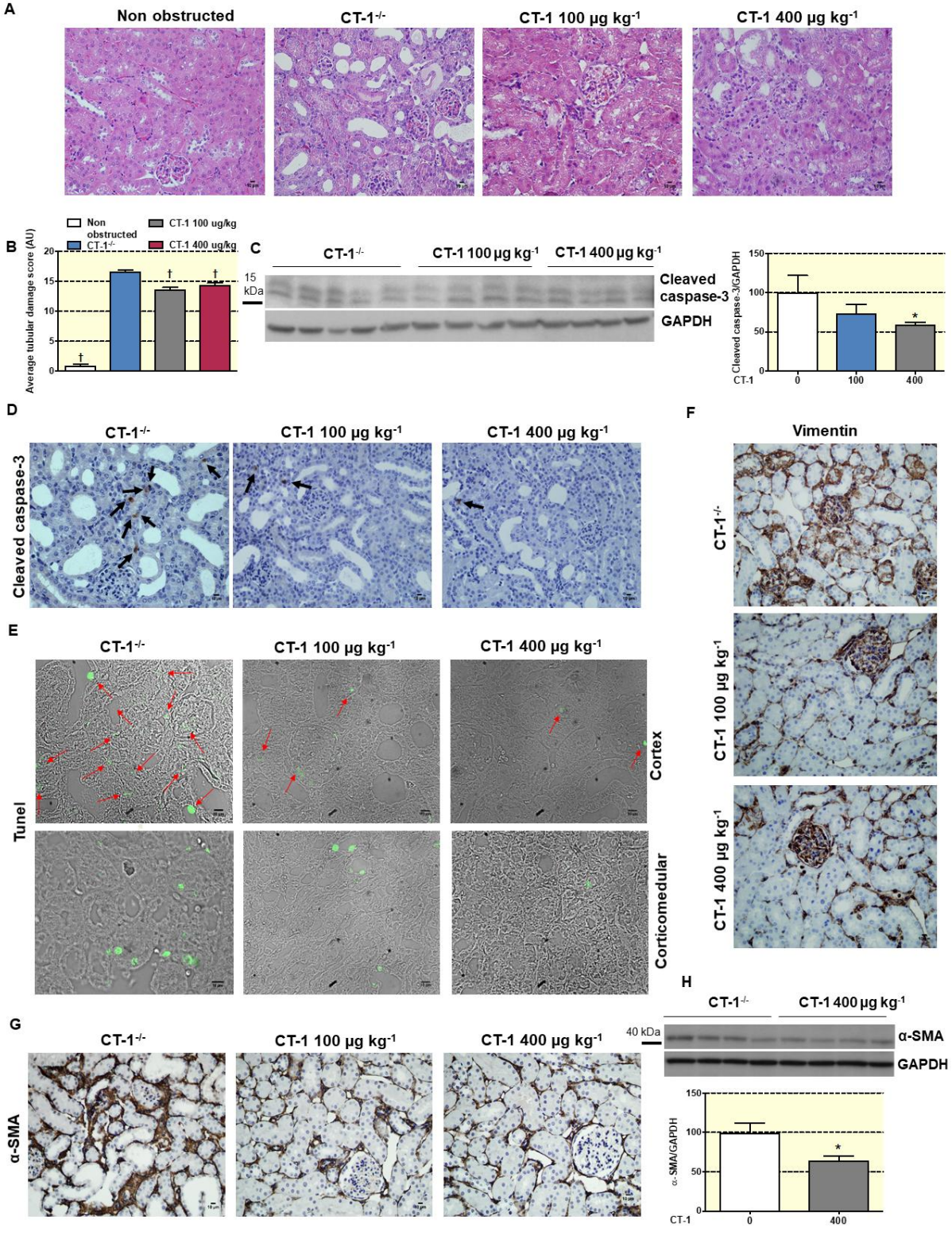

Figure 6

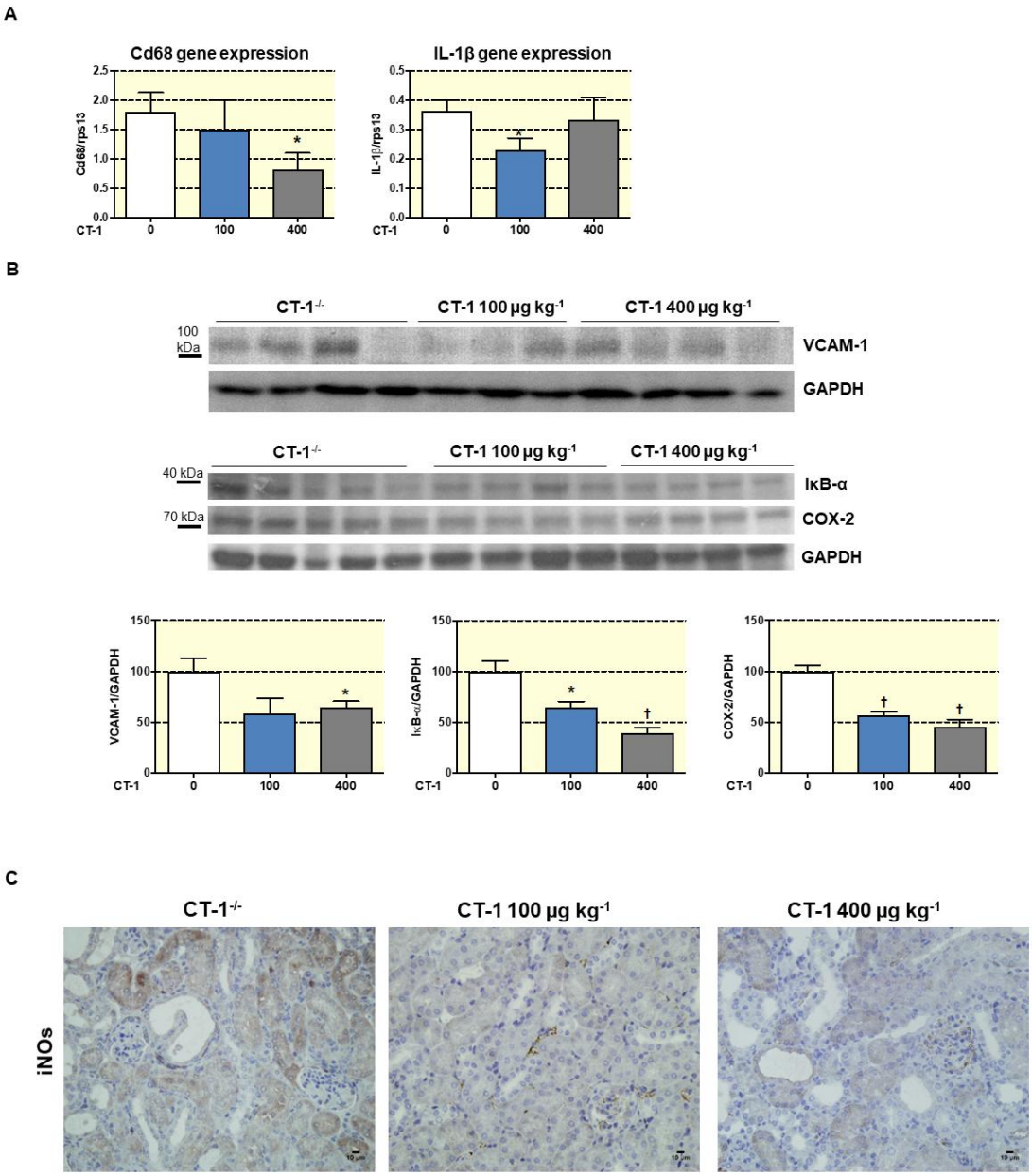

Figure 7

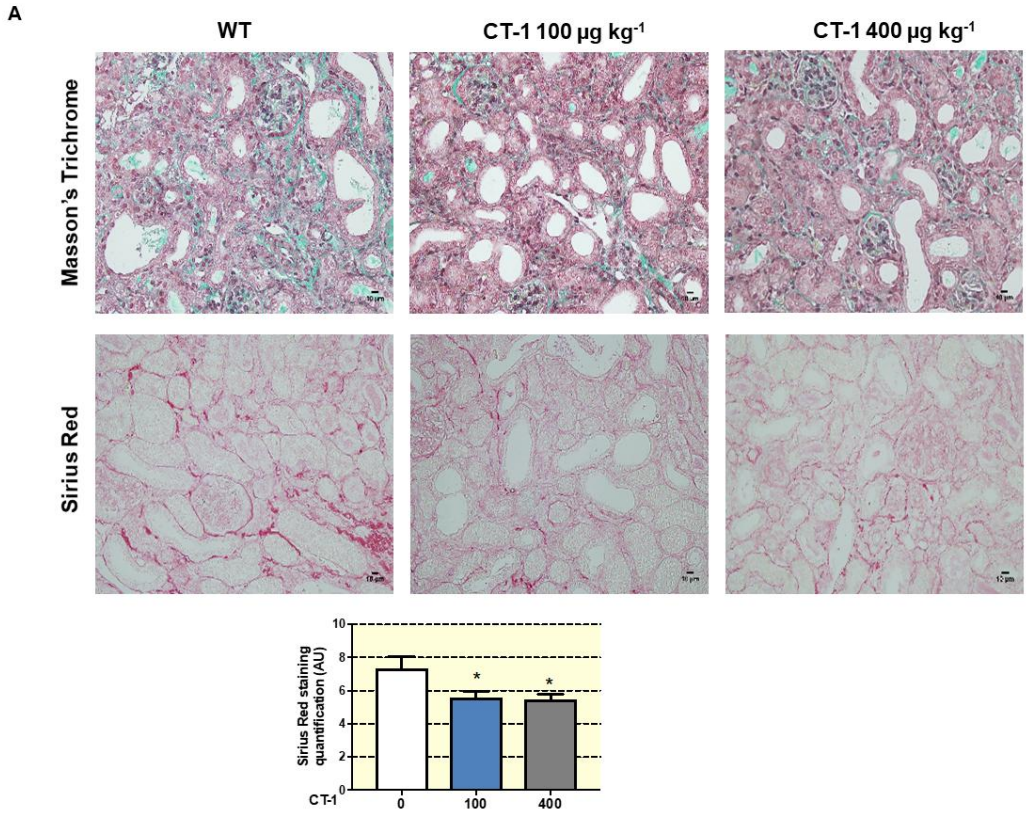

Figure 8

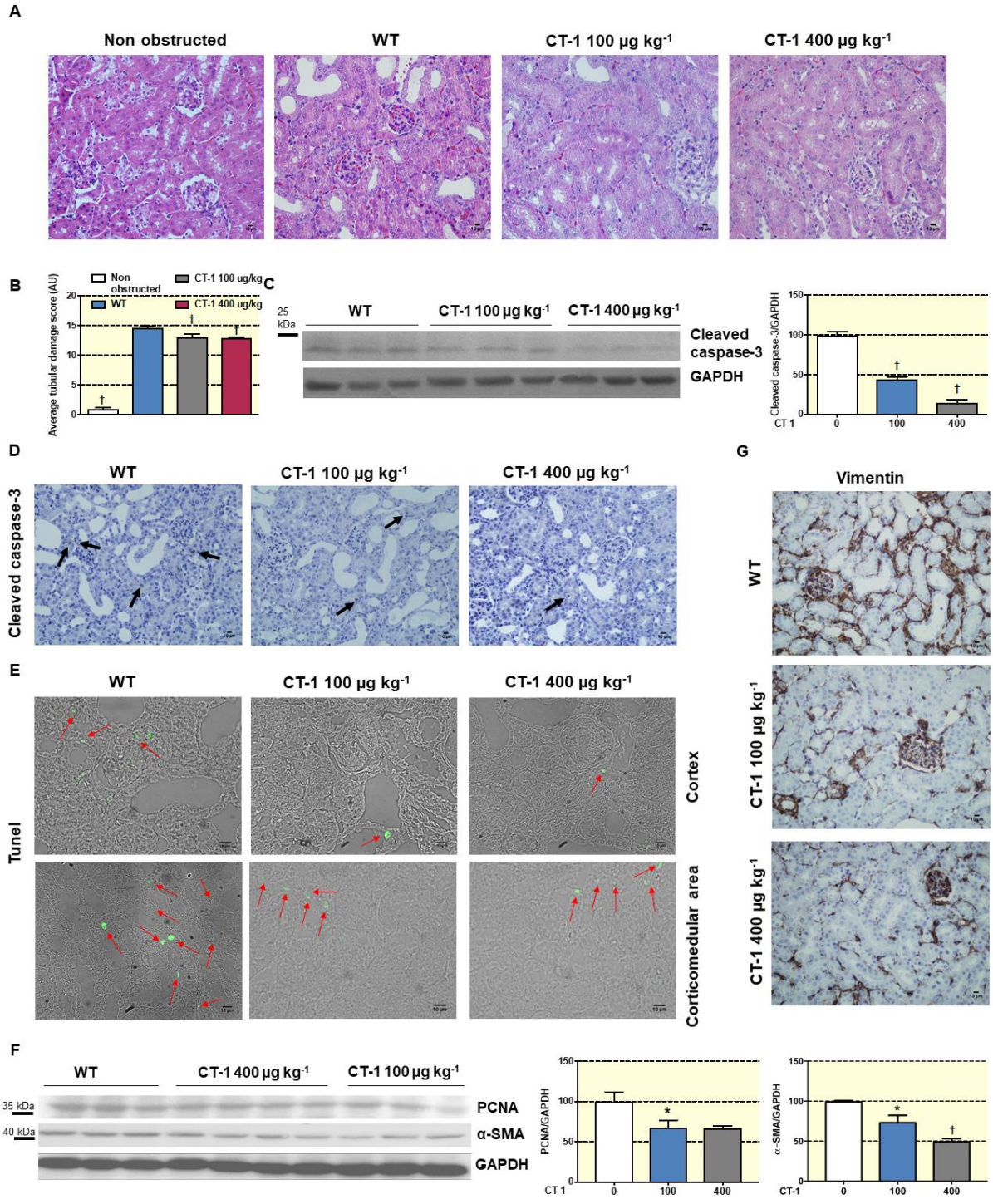

Figure 9

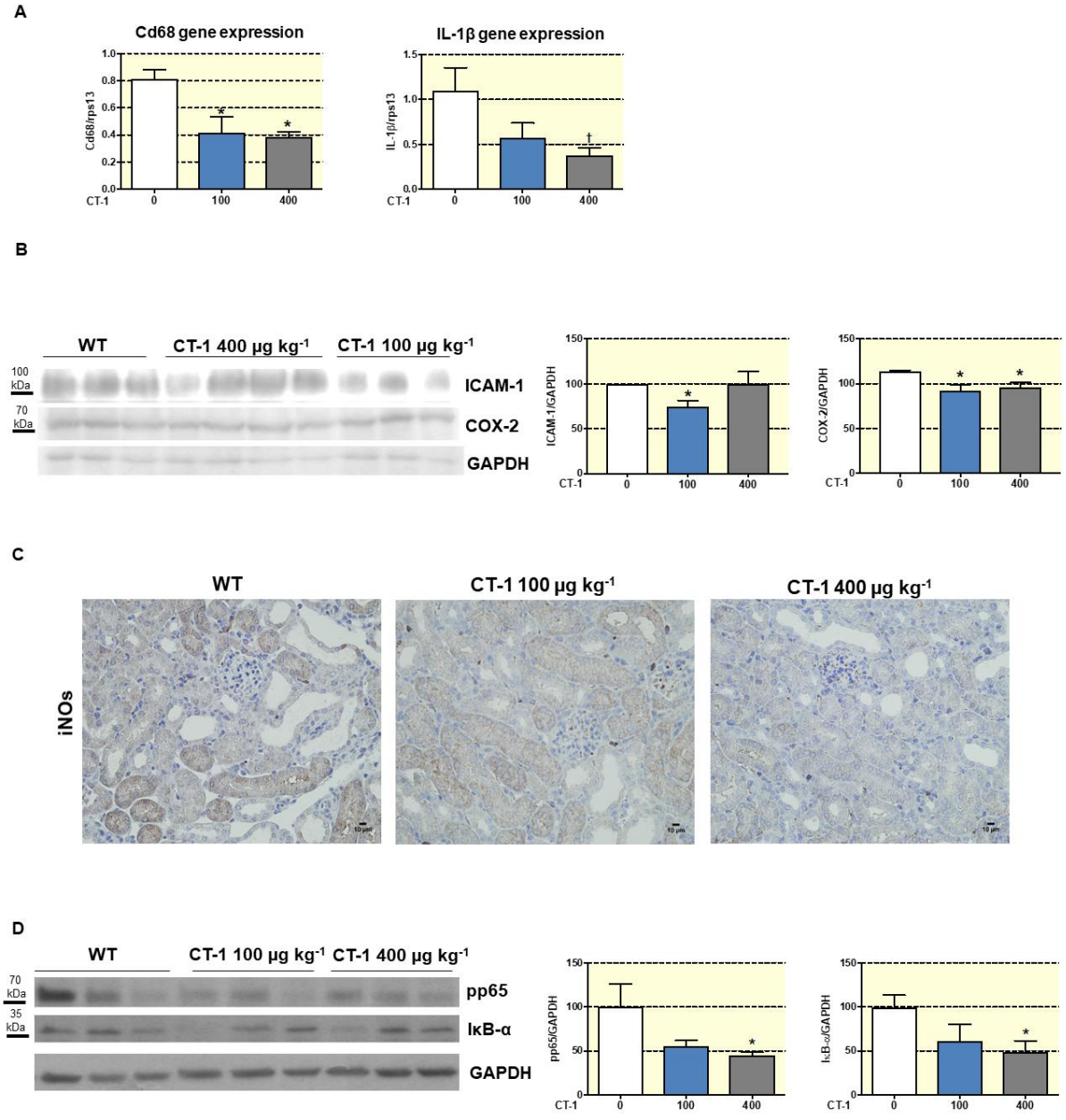

Figure 10